The influence of electrodeposition potential on the chemical composition, structure and magnetic properties of FeCoNi nanowires

Anna Nykiel, Piotr Ledwig, Piotr Pawlik, Jaafar Ghanbaja, Grzegorz Cempura, Adam Kruk, Alain Walcarius, Malgorzata Kac

The influence of electrodeposition potential on the chemical composition, structure and magnetic properties of FeCoNi nanowires

Anna Nykiel[1,2]*, Piotr Ledwig[3], Piotr Pawlik[4], Jaafar Ghanbaja[5], Grzegorz Cempura[3], Adam Kruk[3], Alain Walcarius[2] and Malgorzata Kac[1]*

[1]*Institute of Nuclear Physics, Polish Academy of Sciences, PL-31342 Kraków, Poland*

[2]*Universite de Lorraine, CNRS, LCPME, F-54000 Nancy, France*

[3]*AGH University of Science and Technology, PL-30059 Kraków, Poland*

[4]*Częstochowa University of Technology, PL-42200 Częstochowa, Poland*

[5]*Universite de Lorraine, CNRS, IJL, F-54000 Nancy, France*

Abstract

FeCoNi nanowires with diameters of 30 nm and 100 nm and a length of 6 µm were electrodeposited in the polycarbonate membranes at constant cathodic potentials ranging from -1.0 to -1.8 V. The increase in cathodic potential caused an increase in Ni content with a simultaneous decrease in Fe and Co concentrations. The samples showed an fcc structure (with a small hcp fraction observed in one sample) with a preferred growth along [111] direction, which changed to a [220] texture at higher deposition potentials. With the increase in Ni content, a shortening of the lattice parameters and an increase in the crystallite size were observed. Various chemical compositions resulted in the modification of the magnetic properties of nanowires. The magnetization saturation value increased with increasing cathodic potential for both types of nanowires. However, coercivity and squareness rose for samples with a diameter of 30 nm and fell down for 100 nm diameter nanowires. This specific behavior was explained based on dipolar interactions, which can be neglected in 30 nm diameter nanowires, due to the low membrane porosity.

Keywords: nanowires, FeCoNi, template-assisted electrodeposition, anomalous co-deposition, magnetic properties

Introduction

Along with technological progress, manufactured devices are not only more efficient but also smaller and smaller. Entering the nanoscale, appropriate nanostructures such as nanoparticles, nanotubes or nanowires must be used for the production of those devices [1], [2]. Nanowires (NWs) are one-dimensional objects with a diameter of nanometers and micrometric lengths, which due to their cylindrical geometry, exhibit anisotropy of the physical properties and – what is especially important in the case of magnetic nanowires – magnetic anisotropy. Such structures demonstrate a wide range of applications from biomedicine to consumer electronics; for example, they are used in cancer therapy or in drug delivery systems, as MRI contrast agents, [3], [4] or as pressure, gas, liquids and acoustic sensors, in microwave devices or as tips for magnetic force microscope [3], [5]–[12].

Cylindrical magnetic nanowires are also attractive materials for next-generation data storage devices like 3D magnetic memory units with a density of several dozen terabits per square inch [13]–[16]. Current magnetic data storage devices rely on a two-dimensional design. Because of the superparamagnetic behavior observed when the size of the magnetic bits is reduced, density in such storage media cannot be improved. An alternative approach is the constructing of 3D devices in which vertically arranged magnetic domains are used to store information in parallel arrays of tall columns – nanowires. Such nanowires are

embedded in a non-magnetic matrix, thus the individual segments will be deep in the membrane. To extract the information, the domain wall motion along the nanowires should be considered. In 2D objects, the domain wall motion can be achieved by spin-polarized electrical current and/or magnetic field. In the case of magnetic sections arranged in 3D fashion, the domain wall propagation can also be reached by means of spin-polarized current or RKKY (the Ruderman–Kittel–Kasuya–Yosida) interactions [17]–[19]. However, this concept has not been transferred to devices on an applicable scale [17], [18], [20], [21].

The nanowires can be produced by many techniques such as lithography, chemical vapor deposition, ablation or electrochemical deposition. The template-assisted electrodeposition method is often used to produce nanowires due to its versatility and suitability for large-scale production. Also, using this technique, it is possible to obtain the desirable parameters of nanowires, like shape and size [22]–[24]. An additional advantage of this technique is that it is relatively easy to sequentially grow and combine various segments of dissimilar materials exhibiting different physicochemical properties along the nanowire [25].

Parallel arrays of segmented nanowires embedded in a non-magnetic matrix produced by template-assisted electrodeposition technique are exactly the kind of three-dimensional system, which can meet the demands of 3D memory units. The use of multisegmented nanowires requires full control of the orientation of the different magnetic segments. To achieve this goal each magnetic segment should exhibit a well-defined, sufficiently different value of coercivity [25]. The coercivity strongly depends on the geometry of the segments and of course on their chemical composition. For example, the use of the templates with modulated pore size or post-deposition etching of nanowires enables the production of segments with different diameters, which results in a varied coercivity of the particular magnetic parts [15], [16], [26]–[28]. Another idea is to produce segments from materials with different magnetic hardness such as Co and Ni [18] or alloys such as FeCoNi with different chemical compositions.

Well-chosen chemical composition is a factor that affects various parameters, including magnetic properties such as the mentioned coercivity (H_C), but also remanence (M_R), saturation magnetization (M_S) and squareness (M_R/M_S). Studies by Budi *et al.* showed an increase in both M_S and H_C values with an increase in Fe and a decrease in Ni content in the FeCoNi films [29]. Such a chemical modification can be achieved by changes in the cathodic potential in the single-bath electrodeposition process [23], [29], [30]. The chemical composition of FeCoNi alloys determines the phase composition and crystallographic structure, which decide on the magnetocrystalline anisotropy [23], [31][31]. However, it should be noted that only a well-selected electrolyte composition ensures clear changes in the chemical composition of the deposit as a function of the applied potential [28].

In addition, alloys from the iron group show an anomalous deposition type, which means that less noble metal atoms are deposited preferentially over more noble atoms despite a lower standard potential [29], [32]–[35]. This electrodeposition process is complicated because the reduction of those elements occurs not only from Fe^{2+}, Co^{2+} and Ni^{2+} but also from the corresponding metal hydroxide ions ($FeOH^+$, $CoOH^+$ and $NiOH^+$), which show larger reaction rate constants than in the case of the free ions [36]. The possible explanation for principal features of anomalous co-deposition is based on the hypothesis that in iron-group metal the electrodeposition of the metal hydroxide ions, MOH^+ (M = Co, Ni, Fe), are the primary precursors competing with each other for surface sites at the electrode [36], [37]. Inhibition of the electrodeposition of more noble elements is assumed to result from preferential coverage in order: $FeOH^+ > CoOH^+ > NiOH^+$, due to the differences in kinetics [38]. Although there are models that elucidate the anomalous

phenomena for coatings [24], [33], the mechanism of FeCoNi nanowires deposition into the porous matrix is still an open question.

The type of deposition is highly dependent on the parameters of the electrolyte and the electrodeposition process, especially on the concentration, pH, temperature and applied potential [33]. Budi *et al.* reported that in the case of FeCoNi films (*i.e.* not nanowires), the features typical of anomalous co-deposition clearly attenuated at more negative potentials [29]. This means that by changing the cathodic potential it is possible to control the type of deposition and, consequently, the chemical composition of the obtained materials. The anomalous co-deposition can also occur when atom crystallization is hindered because the atom solubility limit is lower than the ion concentration in the electrolyte [31].

The type of the electrodeposition process can be determined using the selectivity ratio (SR) parameter, which is defined as the atomic ratio in the deposited material to the molar ratio in the initial electrolyte [24], [33]. Dragos et. al. showed that the obtained values are in the range from 1 to 15, where 1 stands for standard deposition, while 15 informs about anomalous co-deposition, but in general, it can be assumed that the higher the SR coefficient, the more anomalous co-deposition is [33].

Besides chemical composition, the magnetic properties can be modified by the geometrical parameters of nanowires such as diameter, length and inter-wire distance [39]. The decrease in the diameter and length usually (not always [40], [41]) causes an increase in the coercivity and squareness [39], [42]. It can be explained by the smaller influence of the dipolar interactions between neighboring nanowires [42]–[48]. The main geometrical parameter that characterizes nanowires is an aspect ratio defined as a length (L) to diameter (ϕ). This parameter affects the shape anisotropy [49], [50], which aligns the magnetization vector along the nanowire axis and causes the coercivity to increase to an aspect ratio value of about 10 or more and then due to the increasing role of the magnetostatic interaction, coercivity reduces significantly [39], [42], [49], [51]. Another important parameter is related to the nanowire quality. The more defected nanowires may be a reason for the larger coercivity because of the domain wall pinning caused by structural defects and other nanowire imperfections [51], [52]. Such an effect can be reached by applying different potentials, which affect the deposition rate and result in the changes in the nanowire morphology observed in the form of a decrease in the membrane filling degree [51], [52]. A defected structure can be also reached by using electrolytes with a very low pH, which causes high hydrogen evolution leading to the formation of nanostructures with high porosity [53]. In addition, there is also the membrane porosity, which determines the inter-wire distance and for low porosity it can be large enough to weaken the magnetostatic interaction between the nanowires, resulting in an increase in coercivity and squareness [47]–[49], [54]–[56].

Thus, to meet the criteria required for 3D magnetic memory media, magnetic nanowires with well-defined parameters like coercivity and remanence are required. Additionally, the nanowires should be homogenous and smooth enough to enable domain wall motion and should be well separated to reduce inter-wire interactions.

In this paper, we investigated the electrochemical generation of homogenous FeCoNi nanowires grown at different cathodic potentials in porous polycarbonate membranes. The materials obtained in this way, characterized by different chemical compositions, allowed the production of nanowires with different magnetic properties. The influence of phase composition and microstructure on the magnetic properties of nanowire arrays will be explored here, with a view to their possible use as a candidate for 3D magnetic memory media.

Materials and methods

FeCoNi nanowires were electrodeposited in polycarbonate membranes with the vaporized copper or gold contact layer (sputtering), which closed the pores from one side and acted as a cathode. The membranes with a nominal thickness of 6 µm and pore diameter of 30 nm and 100 nm showed inhomogeneous pore distribution with a density of approximately 6 x 10^8 pores/cm^2 and 4 x 10^8 pores/cm^2, respectively [57]. The electrodeposition process was performed in an electrochemical cell in a three-electrode system with a metal-coated membrane as working electrode and with Ag/AgCl wire and platinum sheet as reference and counter electrode, respectively. The electrodeposition process was controlled by the AUTOLAB PGSTAT302N potentiostat (Metrohm Autolab B.V., Utrecht, The Netherlands) operating in the potentiostatic mode with the applied cathodic potential varying from -1.0 V to -1.8V vs. Ag/AgCl. The deposition was carried out in an electrolyte bath containing Fe^{2+}, Co^{2+} and Ni^{2+} ions from their sulfate salts with the addition of boric acid (to stabilize pH extending the region of proton reduction to more negative potentials and avoiding metal hydroxide precipitations [58]) and ascorbic acid (to prevent iron oxidation by residual oxygen). The detailed electrodeposition conditions with electrolyte composition are presented in Table 1. The processes were stopped when a sudden increase in the cathodic current informing on the full pore filling was recorded. Moreover, the coatings with a thickness of about 10 µm were prepared on the thin copper foil at the same electrodeposition conditions.

Table 1. The detailed electrodeposition conditions with electrolyte composition.

Electrolyte composition	[g/L]:	[mol/dm^3]
$FeSO_4$	2.78	0.01
$CoSO_4$	5.62	0.02
$NiSO_4$	44.71	0.17
H_3BO_3	40	0.65
$C_6H_8O_6$	1	0.006
pH	3.0	
Temperature [°C]	25	

The full membrane filling was confirmed by microscopic surface observation using the scanning electron microscope (SEM) Tescan Vega 3. SEM was also used for observing the nanowires after membrane dissolution in dichloromethane. The structure of nanowires (and flat samples) was studied by X-ray diffraction (XRD) using a Philips X'Pert MRD Pro diffractometer with Cu Kα radiation. The samples were also analyzed using a transmission electron microscope (TEM) FEI Titan Cubed G2 60-300 microscope (FEI) equipped with the ChemiSTEM system and also a JEM - ARM 200F Cold FEG TEM/STEM operating at 200 kV and equipped with a spherical aberration (Cs) probe and image correctors. Scanning transmission electron microscopy (STEM) images were acquired using a high-angle annular dark-field (HAADF) detector. The STEM-EDS data was analyzed by Esprit software (Bruker) in which the standardless Cliff-Lorimer quantification method was used. Indexing of electron diffraction patterns was performed with the use of JEMS software. The chemical composition of the coatings and nanowires was studied by energy-dispersive spectroscopy (EDS) measurements performed in SEM and STEM. The magnetic properties of nanowires were measured at room temperature in two directions with an external field of up to 4T applied in the plane and out of the plane of the membrane, using a Quantum Design MPMS superconducting quantum

interference device magnetometer (SQUID). The diamagnetic signal coming from polycarbonate was subtracted from the curves.

Results and discussion

The FeCoNi nanowires were grown by potentiostatic electrodeposition into the polycarbonate membranes with diameters of 30 nm and 100 nm by applying various cathodic potentials. Before investigating the effect of the electrochemical parameters on the morphology as well as the chemical, structural and magnetic properties of nanowires, some preliminary voltammetric characterizations were performed.

Cyclic voltammetry

Cyclic voltammetry (CV) was first used to help select the electrodeposition parameters and to better understand the cathodic behavior of the metal species. CV as a powerful technique to analyze electron transfer-initiated chemical reactions can also turn out to be a helpful tool in studying anomalous co-deposition mechanism.

CV measurements of solutions containing $FeSO_4$, $CoSO_4$ and $NiSO_4$ electrolytes were first performed separately to obtain initial information about the deposition process and define the potential regions where the cathodic deposition starts. The corresponding voltammograms recorded at a scan rate of 10 mV/s in a potential window between -1.2 V and 0.2 V (or 0 V for Fe) are shown in Figure 1.

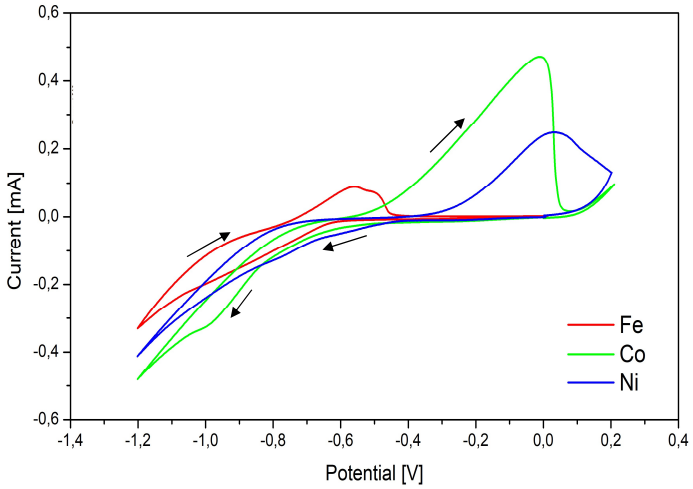

Figure 1. Cyclic voltammograms recorded in an aqueous solution containing separately $FeSO_4$, $CoSO_4$, or $NiSO_4$ (50 mM) in 0.65 M boric acid and 5.7 mM ascorbic acid, at a potential scan rate of 10 mV/s using a gold electrode.

In all measurements, the potential scan started in the cathodic direction from 0 V, without any noticeable current response until about -0.4 V, and then some ill-defined cathodic waves appeared as a consequence of the slow reduction of metal ions, according to the progressive nucleation mechanism, as respectively reported for the electrodeposition of iron [59], cobalt [60], and nickel [61]. Consistent with previous observations on reduction potentials [62], the deposition of nickel occurred first at less cathodic potential values, then cobalt followed by iron at more negative values. Although no distinct peaks can be detected, it is clearly seen that this order of reduction potential is in agreement with the standard potentials (-0.44

V for Ni^{2+}/Ni, -0.47 V for Co^{2+}/Co, and -0.64 V for Fe^{2+}/Fe, vs. Ag/AgCl). For cobalt, one can even notice two successive reduction waves, consistent with the previous report on cobalt electrodeposition on polycrystalline gold electrode [63]. Below -1.1 V, the current rapidly rose due to hydrogen evolution. On the scan reversal, one can clearly see a metal dissolution in the form of well-defined anodic stripping peaks appearing in the reverse order of metal cation reduction confirming that metallic deposits were indeed formed during the cathodic scan. Stripping peaks were however asymmetric, with slow current increase suggesting rather slow dissolution processes.

When present in a mixture ($FeSO_4$ + $CoSO_4$ + $NiSO_4$), the electroreduction is expected to form FeCoNi alloys [29], [64]. The corresponding voltammograms recorded at various potential scan rates are shown in Figure 2. One can observe once again ill-defined reduction waves with larger intensities by increasing scan rates, but one cannot distinguish the individual contributions of each metal ions (in spite of this, it is expected that the FeCoNi alloy is indeed produced [62], [64]. On the scan reversal, the stripping peak currents were found to decrease slightly (and thus the charge below the peak decreased even more rapidly) when the potential scan rates rose, indicating that mass transport is clearly not the dominant factor and that the electron transfer kinetics is the rate-limiting step of the electrodeposition process [64].

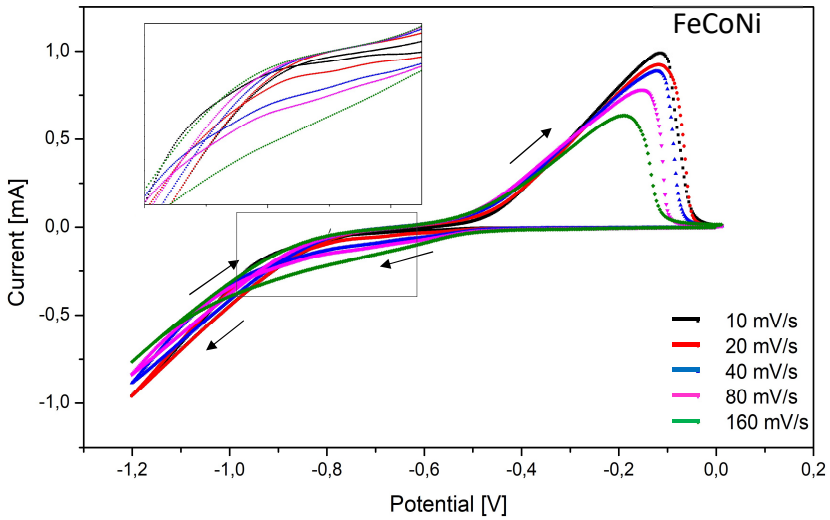

Figure 2. Cyclic voltammograms recorded in an aqueous solution containing $FeSO_4$, $CoSO_4$, and $NiSO_4$ in a mixture (50 mM each) in 0.65 M boric acid and 5.7 mM ascorbic acid, at various potential scan rates (from 10 to 160 mV/s) using a gold electrode.

Compared to the electrodeposition of single metals (Fig. 1), the onset of alloy deposition moved towards lower values of potential (especially for Co^{2+} and Ni^{2+} reduction, Fig. 2). This is an indication of anomalous co-deposition, in which the electrodeposition of less noble element is preferentially deposited because the evolution of hydrogen resulted in an increase in the concentration of hydroxyl ions [65], as observed for the co-electrodeposition of several metal alloys [66]–[68]. It also means that the reduction of the deposited metals strongly depends on the cathode potential and, based on that consideration, it can be stated that varying the electrode potential would enable controlling the type of deposition and, consequently, the chemical composition of the obtained materials not only in thin films [29] but hopefully also in nanowires (as investigated below).

Electrochemical analysis of FeCoNi nanowire growth

Chronoamperometry was used to produce the nanowires by electrochemical reduction of metal ions leading to material growth in a porous membrane. The method involves the application of a constant cathodic potential, causing a current flow and concomitant material deposition. Chronoamperometry was conducted at four different potentials from -1.0 V to -1.8 V using the membranes with two distinct pore diameters: 30 and 100 nm. During the electrodeposition processes, the current variations over time were measured (Fig. 3). The experiments were stopped when the currents suddenly started to grow, which means that the nanowires had reached the upper surface of the membrane [39], [52], [69], [70].

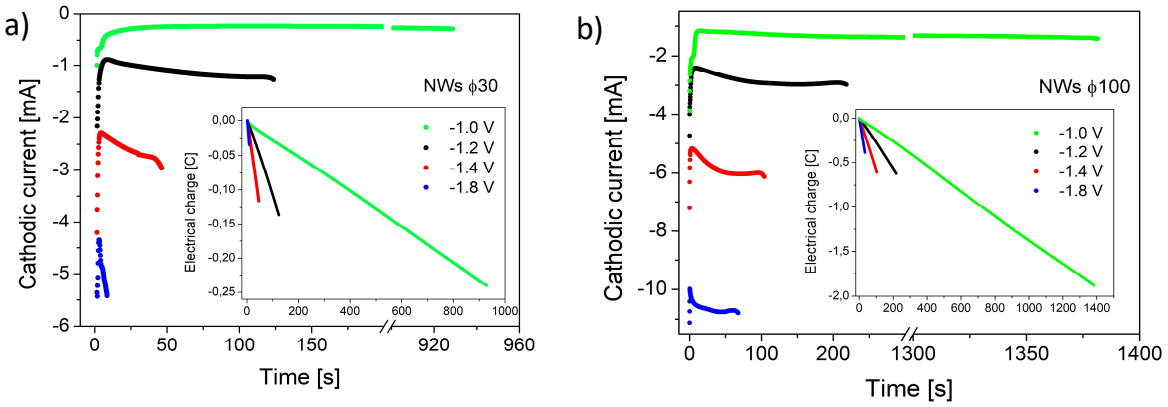

Figure 3. Variation of cathodic currents as a function of time, as measured during the electrodeposition of FeCoNi nanowires at different applied potentials (in conditions as specified in Table 1) using the membranes with pore diameters of 30 nm (a) and 100 nm (b). The insets show corresponding electrical charge variations in time.

As the applied potential increases, for both pore diameters, the cathodic current increases. Consequently, shorter times are needed for the complete filling of the pore channels of the membranes. The currents observed with the membrane having larger pores are more intense than those sampled at the membranes with smaller pores (Fig. 4).

The corresponding electrical charge variations (see insets in Fig. 3) are linear, suggesting a constant growth of the alloy wires into the pores. For both kinds of membranes, the final charge values (*i.e.*, after pore filling) are almost the same for the medium potentials (-1.2 V, -1.4 V), while the measurements for the extreme values differ significantly. The highest value of electrical charge is achieved for the lowest overpotential (-1.0 V), whereas the lowest charge is measured at the most cathodic potentials (-1.8 V). This may suggest a different degree of membrane filling and was previously observed in Fe nanowires deposited at various temperatures [52], [71].

Changes in the applied potential affect the hydrogen evolution, which increases with the overpotential and decreases with pH and metal ion concentrations [60], [72], [73]. Because the last two parameters are relatively high in our case, we can assume that the hydrogen evolution is mainly induced by high overpotential. At high applied potential the hydrogen bubbles can block the pores and hinder the deposition process, leading to more defected structures with more porous or even discontinuous nanowire forms. This effect should be more pronounced in membranes with smaller diameters, which can

be easily blocked by hydrogen bubbles. This factor together with the different membrane porosity is responsible for the lower charge (0.24 C to -0.035 C) reduced in nanowires with a diameter of 30 nm compared to values ranging from -1.9 C to -0.4 C for 100 nm diameter nanowires.

The value of the applied potential affects the rate of both charge transfer and migration of metal ions, inducing thereby different speeds of electrodeposition. The values of current density and growth rate were presented as a function of applied potentials (Fig. 4). For both pore diameters, an increasing cathodic voltage results in larger values of cathodic current densities and deposition rate. The applied potential has a stronger effect on nanowires with a diameter of 30 nm, wherein this effect is more pronounced at higher overpotential probably due to the high hydrogen evolution. Obviously, an increase in the growth rate shortens the process duration. As a result, the time needed to fully fill the membrane changes from 1380 s to 70 s and from 930 s to 10 s, for nanowires with diameters of 100 nm and 30 nm, respectively.

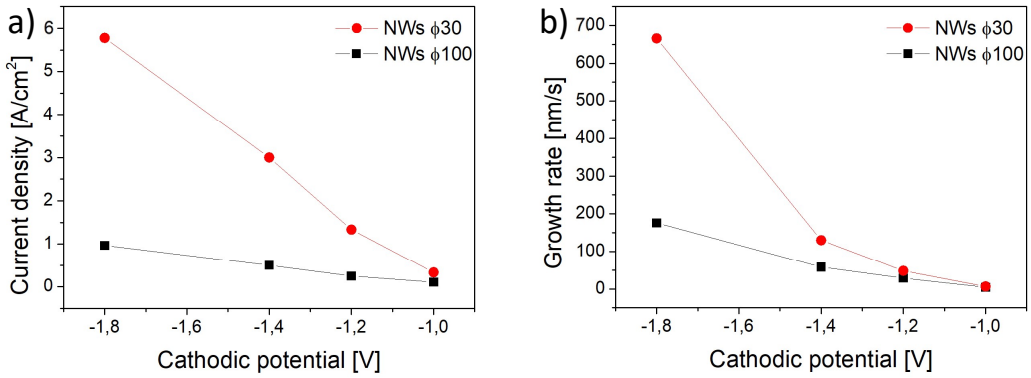

Figure 4. Current density (a) and growth rate (b) measured as a function of cathodic potential for nanowires with a diameter of 30 nm and 100 nm.

Comparing the current and charge plots for both membranes, it can be seen that they show the same relationship, suggesting the same deposition mechanism.

Chemical composition

Different values of the cathodic current recorded for individual elements versus cathodic voltage during the measurement of the cyclic voltammetry allow us to expect different behavior of Fe, Co and Ni ions under the applied potential. Taking into account literature reports, various standard potentials and observed in this system anomalous co-deposition, we chose the ion concentrations in the electrolyte that should induce changes in the chemical composition of nanowires measured at various potentials [29], [23], [74].

The chemical composition was analyzed using energy-dispersive spectroscopy measurements on the nanowires released from the membranes and on the flat samples. The fractions are given in the atomic concentrations. The concentrations of Fe, Co and Ni in the FeCoNi nanowires with diameters of 30 nm and 100 nm and in the flat samples, deposited at different cathodic potentials are plotted in Fig. 5. All samples show the same tendency with increasing cathodic potential, demonstrating an increase of Ni content with

a simultaneous decrease in Co and Fe concentration, which is consistent with literature data [29], [74]–[77]. For samples deposited at potentials ranging from -1.2 V to -1.8 V, the atomic concentration in the deposits reflects the ion concentration in the electrolyte. Therefore, the mass transfer associated with the number of ions in the electrolyte is much greater for Ni^{2+} than for Fe^{2+} and Co^{2+} ions, which allows to overcome the anomalous co-deposition tendency favoring opposite deposition order (firstly Fe then Co and Ni). The chemical composition of the samples deposited at -1V differs significantly from each other. The flat sample shows a concentration ratio relatively close to the electrolyte composition, while in nanowires concentration of individual atoms clearly deviates from the electrolyte and order predicted by standard potential values. The main difference between porous templates and a flat sample is related to the diffusion length. As shown by Saedi *et al.* in their studies of FeCoNi nanowires deposited in membranes with different pore lengths (and unfortunately also different diameters) [35], metals with lower concentrations in the electrolyte appear in higher concentrations in the nanowires when the pore lengths are shorter. The authors explain this behavior with a shorter diffusion length, which creates more favorable conditions for the competition of low-concentration ions (Fe and Co) with high-concentration ions (Ni). Diffusion length can also explain the difference in the chemical composition of elements in the membrane pores and on the flat sample. By analogy, a lower deposition rate (at low cathodic potential) also creates more favorable conditions for very diluted ions, which may result in a higher concentration of them in the deposit. At a more cathodic potential mass transport limitation connected with low ion concertation dominates and metal with high concentration is preferentially deposited [35], [78]. Despite the large difference in the concentration of individual ions in the electrolyte (0.01 M Fe^{2+} / 0.02 M Co^{2+} / 0.17 M Ni^{2+}), the amount of the elements in nanowires at this potential is similar to each other and shows a relatively high concentration of Fe and a clear dominance of Co. This behavior of nanowires indicates anomalous co-deposition, which is not usually observed at more cathodic potentials [29], and suggests that the mechanism of anomalous co-deposition in nanowires can be more complicated than in flat samples.

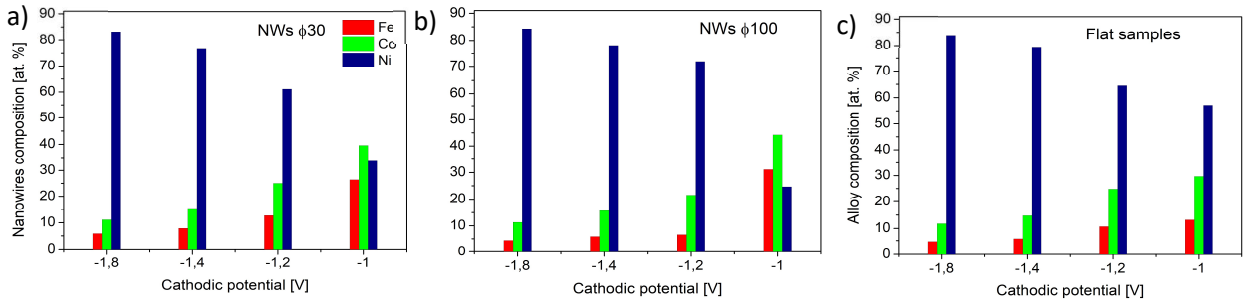

Figure 5. Atomic composition of Fe, Co, Ni in FeCoNi nanowires with diameters of 30 nm (a) and 100 nm (b) and in FeCoNi films (c) deposited at different potentials. The particular elemental contents were given with an error of no more than ±1.

The chemical composition of nanowires with a diameter of 30 nm and 100 nm was also locally analyzed using a scanning transmission electron microscope. The EDS maps measured for Fe, Co and Ni are presented in Fig. 6. The images show a homogenous distribution of the elements. The results demonstrate

the same tendency in the atomic concentration values as a function of the applied potential and correlate very well with the compositions obtained in SEM.

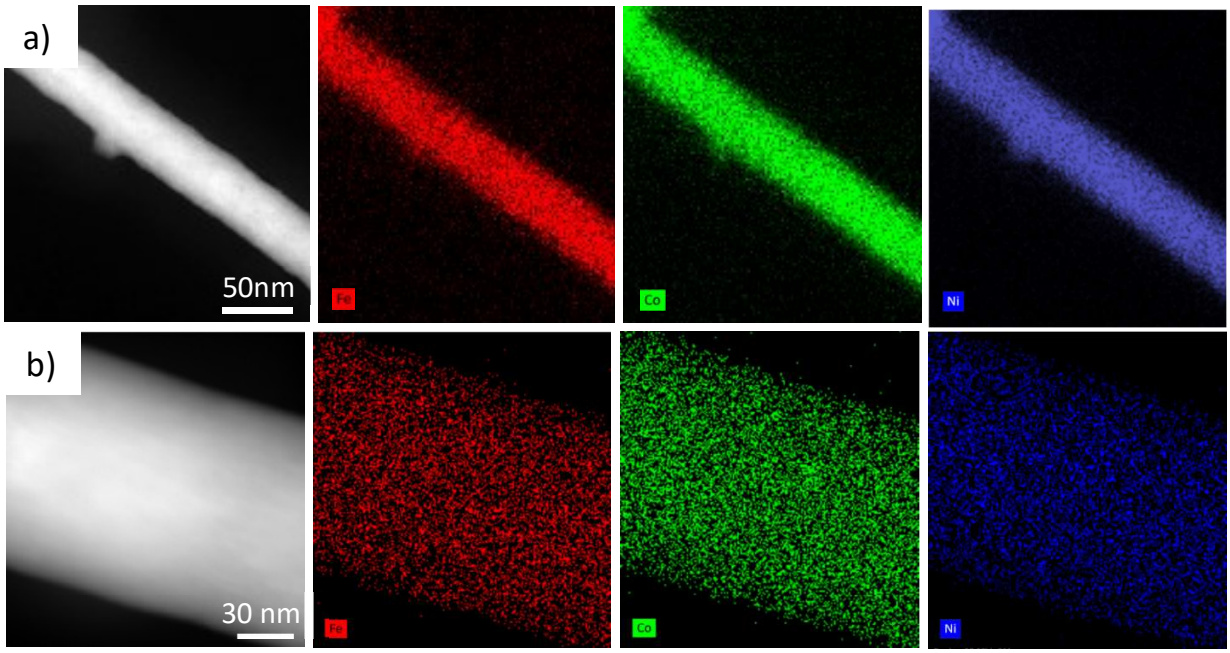

Figure 6. The STEM-EDS maps of Fe, Co and Ni measured for 30 nm (a) and 100 nm (b) diameter nanowires deposited at -1.2 and -1.0 V, respectively.

To better describe the interrelationships between the elements and in order to try to understand the influence of each element on the other two, we calculated SR parameters for Co/Fe, Fe/Ni and Co/Ni ratios as a function of applied potential (Fig. 7). This parameter relating atomic concentration ratios to their molar ratios in the electrolyte allowed Dragos *et al.* to evaluate the extent of anomalous co-deposition [33]. The SR value close to 1 suggested co-deposition predicted by standard potentials and electrolyte composition, while anomalous co-deposition occurred for a higher SR coefficient [33].

The calculations demonstrated similar behavior of particular ratios versus voltages, as expected from chemical analysis, but there are some details that stand out. The first is the SR parameter calculated for the Co/Fe ratio, which maintains an almost constant value for all potentials and samples with a value close to 1. The second issue is the parameters calculated for Ni/Fe and Ni/Co ratios, which show the same values for higher potentials (close to 1) with a sharp increase in SR at lower voltages. Additionally, these parameters reach the largest values for nanowires with a diameter of 100 nm and the smallest for flat samples. The above analysis reveals that the concentration of Fe and Co weakly depends on the applied potential, which is also confirmed by research on FeCo nanowires (paper in preparation). On the other hand, the results point out a strong potential dependence of the Fe/Ni ratio, which was also observed in our studies on binary FeNi nanowires (paper in preparation). Similar results were obtained for FeCoNi nanowires [76], [80] and for FeCo and FeNi nanowires [35], [79]. The behavior of the SR parameter calculated for Co/Ni is consistent with the changes in Fe/Ni, which suggests that the concentration of Ni is very sensitive to the applied potential and plays a dominant role in the anomalous co-deposition mechanism. As was mentioned above, anomalous co-deposition depends on the applied voltage and at high cathodic overpotential, the electrodeposition process loses its anomalous character (Fig. 7). A

significant anomalous co-deposition only appears at the lowest potential, which is in accordance with direct observation of EDS measurements (Fig. 5). The difference between the SR parameters observed for nanowires and flat samples indicates less anomalous co-deposition for flat samples, which confirm a distinct mechanism for anomalous co-deposition in nanowires and coatings.

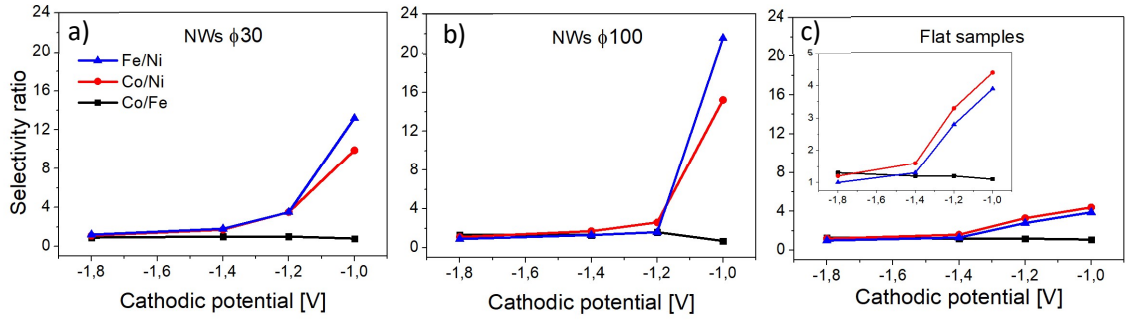

Figure 7. Selectivity ratios of Fe/Ni, Co/Ni and Co/Fe calculated for FeCoNi nanowires with diameters of 30 nm (a), 100 nm (b) and for FeCoNi flat samples (c) deposited at different potentials. The inset shows the same graph on a larger scale.

As reported by Mansouri, an anomalous co-deposition has a direct impact on the final composition of the iron group alloys and, consequently, on their structural and magnetic properties (coercivity, squareness, etc.), which will be the subject of analysis in subsequent parts of the work [80].

Morphology and structure

As mentioned above, all electrodeposition processes were stopped after the pores were completely filled, which was indicated by a drop in the current curve. SEM images confirmed that the nanowires reached the membrane surface and the processes were finished before they expanded in the form of overdeposited caps (Fig. 8).

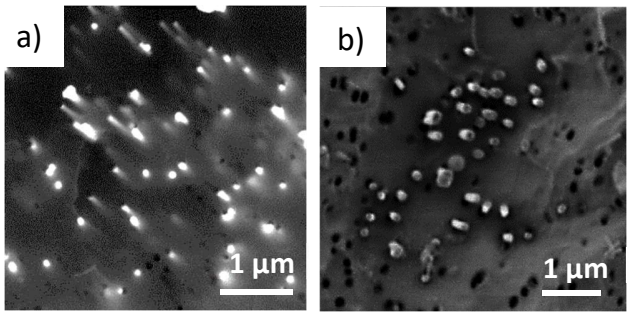

Figure 8. Scanning electron microscopy images acquired on the membrane surface with a pore diameter of 100 nm that do not show overdeposited nanostructures, prepared at a cathodic voltage of -1.2 V (a) and -1.4 V (b).

To observe the morphology of nanowires, polycarbonate membranes were dissolved. SEM images show that there are no significant differences between the nanowires deposited at various potentials (Fig. 9).

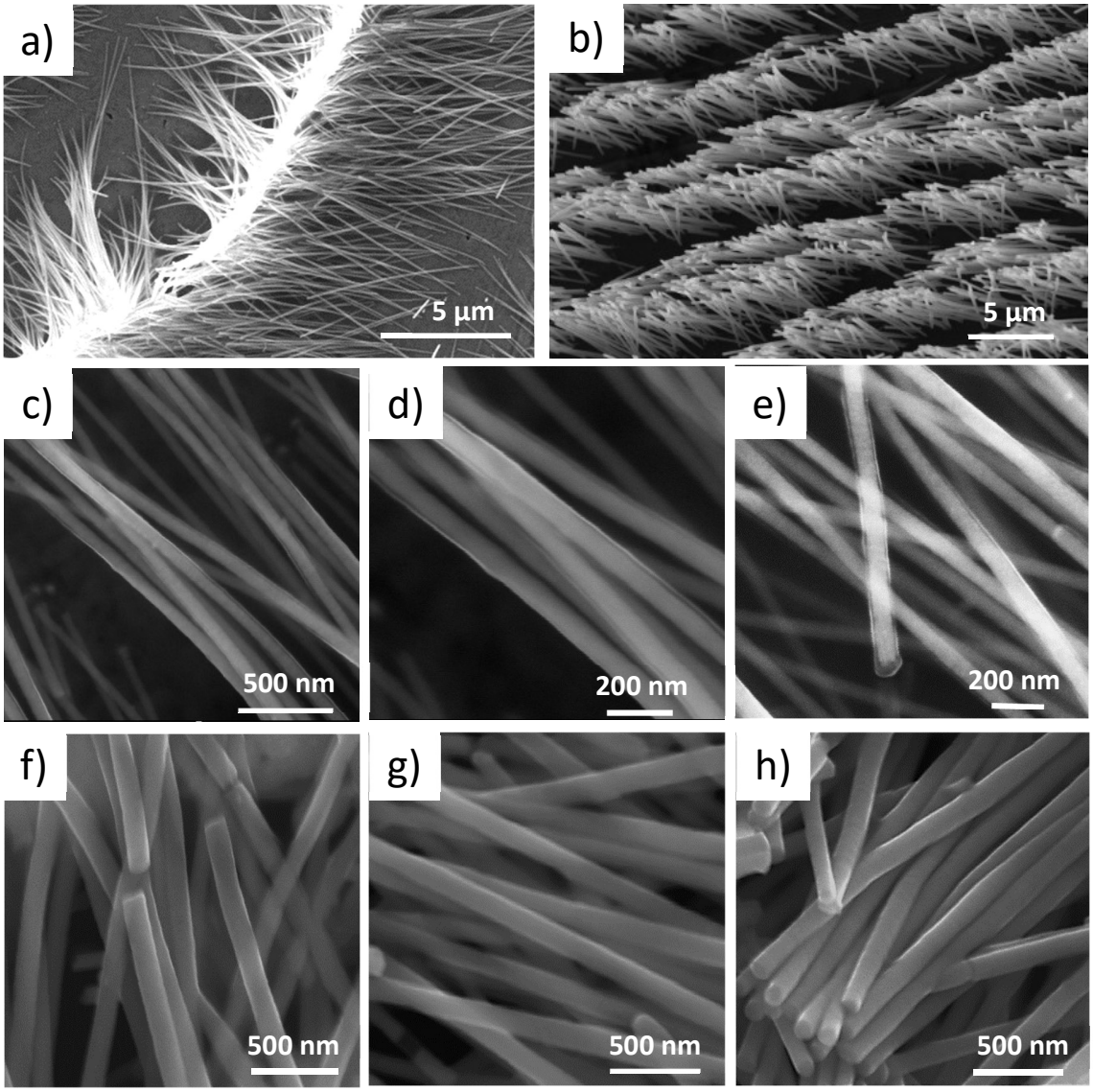

Figure 9. SEM images of the FeCoNi nanowires with diameter of 30 nm (a, c—e) and 100 nm (b, f—h) deposited at the different potentials observed after membrane dissolution: 30 nm of diameter: -1.2 V (a), -1.0 V (c), -1.4 V (d), -1.8 V (e); 100 nm of diameter:-1.2 V (b), -1.0 V (f), -1.4 V (g), -1.8 V (h).

In all samples, the nanowires create densely packed forest-like, nanostructures. These vertically oriented structures formed matrices of nanowires with uniform diameters and lengths. All nanowires are smooth and continuous, without noticeable porosity. Moreover, at higher magnification, we can see the coating covering nanowires. As previously reported, this is a polycarbonate layer (Fig. 9 d-e) that protects nanowires against oxidation [52].

The microstructure of the FeCoNi nanowires with a diameter of 30 nm (Fig. 10 a-e) and 100 nm (Fig. 10 f-i) was investigated using transmission electron microscopy (TEM) measurements. The overview TEM images show the uniform diameter nanowires in both cases (Fig. 10 a, g). A thin layer covering the

nanowire surface (Fig. 10a) identified previously as polycarbonate coating was shown on the nanowire with a diameter of 30 nm [52]. The selected area electron diffraction pattern (SAED), taken along the [110] zone axis (ZA), indicates the [111] growth direction of nanowires with a diameter of 30 nm (Fig. 10 a-c). However, the crystallite orientation along the [220] direction, confirmed by the SAED pattern with the zone axis along [111], was also found (Fig. 10 d, e). The SAED pattern measured for 100 nm diameter nanowires exhibits a [112] zone axis indicating the growth direction along [111] with the (111) plane distance of 0.212 nm (Fig. 10 f—i).

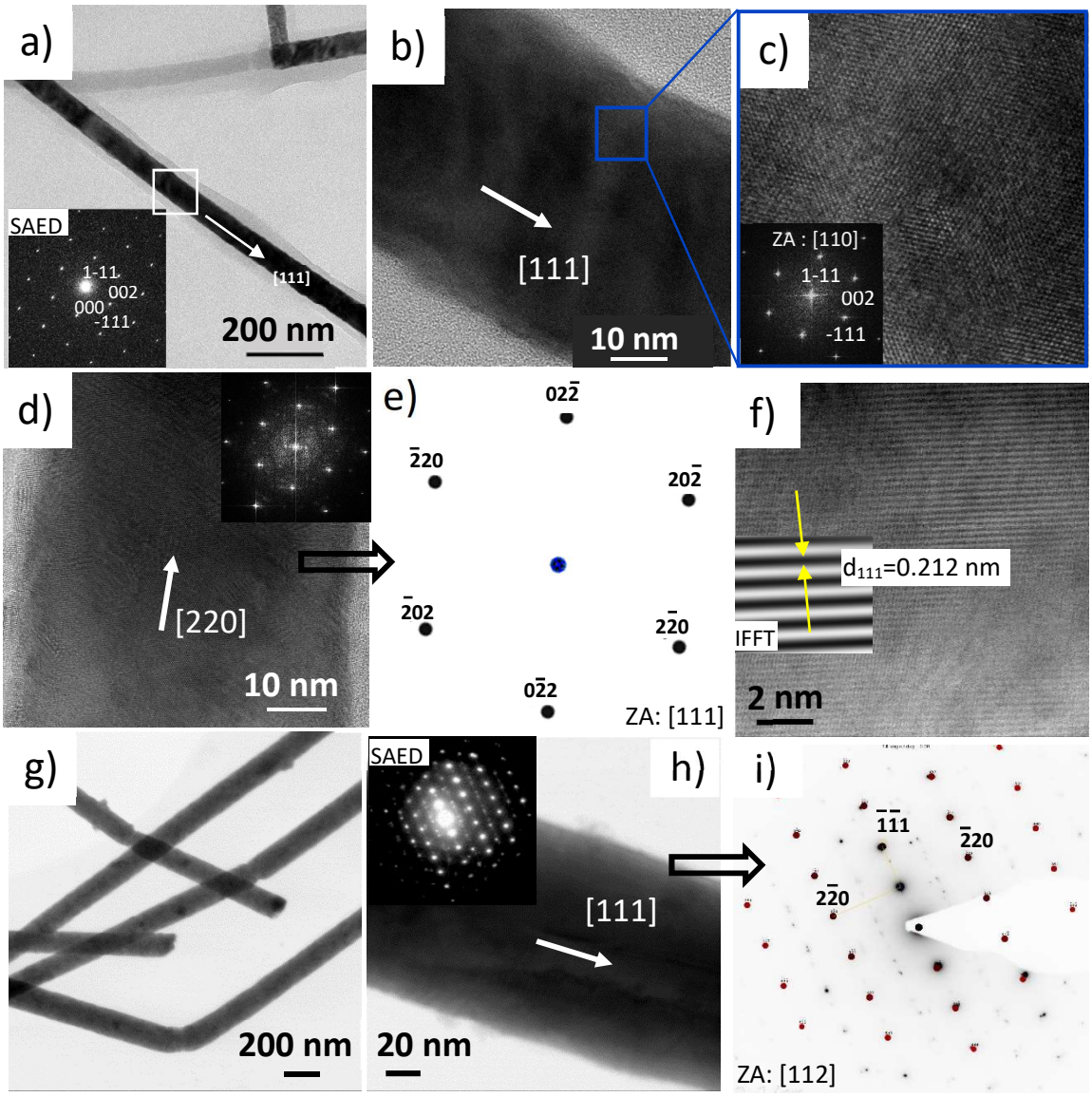

Figure 10. Bright-filed TEM (a, g), high-resolution TEM micrographs (b, c, d) and HAADF STEM images (f, h) of FeCoNi nanowires with a diameter of 30 nm deposited at -1.2 V (a, b, c, d, e) and 100 nm deposited at -1.8 V ((f, g, h, i) together with SAED patterns (a, h, i) and fast Fourier transform (FFT) (c, d) indexed with the lattice parameters of fcc FeCoNi or Ni structure. The (111) inter-plane distance was determined based on the inverse fast Fourier transform (IFFT).

The structure of the nanowires was analyzed based on X-ray diffraction. We present the measurements of nanowires with a diameter of 100 nm (Fig. 11a) and the flat samples (Fig. 11b) deposited at the different potentials. In all samples, the most intense, narrow peaks, marked with an asterisk, originate from the copper contact layer (for nanowires) or substrate (for flat samples). Small peaks at $2\theta = 45.34^{o}$ and $48,71^{o}$ observed in the diffractograms measured for flat samples come from the substrate contamination (marked with triangle-down). The peak intensities were normalized to the (111) peak, which is the most intense in nanowires. The indexed peaks correspond to the FeCoNi phase crystallizing in the fcc structure. These peaks, described in Table 2, appear in all patterns with a slight difference in their position and significantly different intensities.

The diffractograms measured for samples deposited at more cathodic potentials show peaks with higher intensity than the samples prepared at lower potentials. In the case of nanowires, the intensity of the (220) peak increases the most, while in flat samples this observation refers especially to the (200) reflection, which increases even above the (111) peak. These deviations from the intensities observed for isotropic powder samples indicate a texture with a preferential orientation along [220] and [200] directions for nanowires and flat samples, respectively. Simultaneously, the small peak intensities observed for samples deposited at low potentials suggest a texture along the [111] direction in nanowires and quasi-isotropic growth in flat samples.

As shown above, the different values of cathodic potentials caused the changes in the chemical compositions. Such modification in the elemental content should result in a different phase composition. The phases that we can expect in conditions of thermodynamic equilibrium at 293 K are presented in the ternary phase diagram (Fig. 12). Points corresponding to the chemical composition of nanowires with a diameter of 100 nm are marked on the graph. The chemical composition of nanowires with a diameter of 30 nm and flat samples at particular voltages has nearly the same values, except for the -1V potential, for which the points were also shown on the diagram. The samples deposited at potentials ranging from -1.2 V to -1.8 V, showing a Ni content above 70%, are localized in the area where, according to the phase diagram, only the γ-Ni phase should appear. The points showing the chemical concentration of the samples deposited at -1.0 V are localized at two different areas: the points corresponding to nanowires appear in the area where α-Fe, γ-Ni and Ni_3Fe are thermodynamically stable, while the point related to the flat sample occupies the area where the γ-Ni and Ni_3Fe phases should be observed. The α-Fe, γ-Ni and Ni_3Fe phases respectively correspond to the Fe-based solid solution with the bcc structure, Ni-based solid solution with the fcc structure and the $L1_2$ intermetallic phase, which is the ordered counterpart of the fcc solid solution. Ni_3Fe phase, with Fe and Ni atoms located in the corners and on the faces of the unit cell, respectively, is indistinguishable from the disordered Ni phase in the XRD pattern.

In the XRD patterns measured for 100 nm diameter nanowires and flat samples, we only observed peaks that are attributed to the FeCoNi alloys [81], assigned to the γ-Ni phase with an fcc structure. We have not observed any additional peaks that could come from Fe-based solid solution, which should appear in the samples deposited at -1.0 V exhibiting a relatively high Fe content of 31%. The discrepancy between the phase composition predicted by the trinary phase diagram and our nanowires, pronounced especially in the case of the lowest potential, may be explained by non-equilibrium conditions of the electrodeposition process. Similarly, only the fcc phase was observed in FeCoNi alloys with various concentrations by many researchers [81], [82] [83] [77], [84] [74], [85]. Although, the mixture of fcc and bcc [42], or fcc and hcp has also been observed [86] [87]. These differences in the phase composition of the FeCoNi alloy indicate a strong dependence of the growth process on the electrodeposition parameters, which results in a

different structure of the alloy despite a similar chemical composition or an identical structure observed for alloys with different chemical compositions.

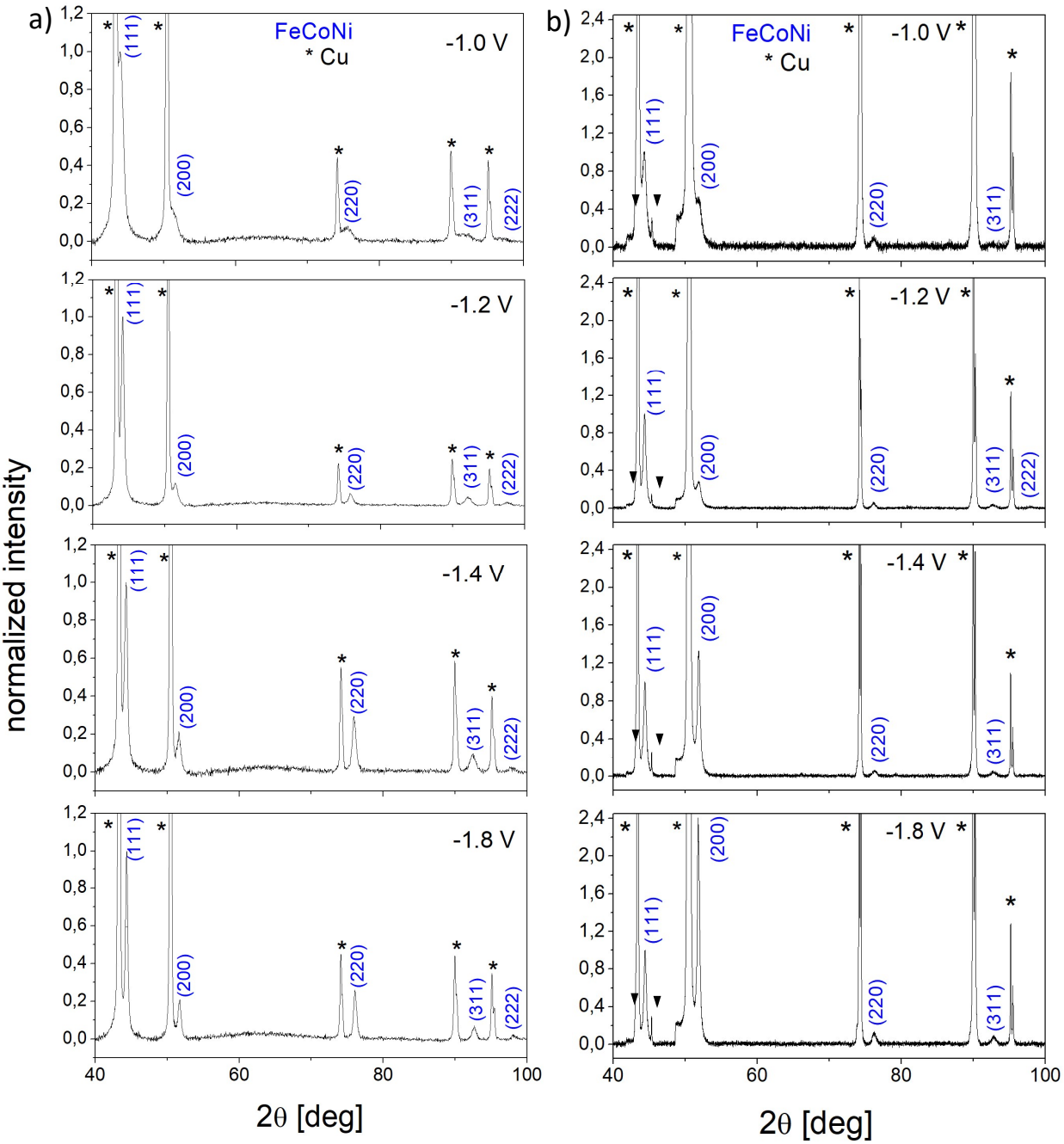

Figure 11. X-ray diffraction patterns measured for the FeCoNi nanowires with a diameter of 100 nm embedded in the polycarbonate membranes (a) and flat samples (b). The indexed peaks correspond to the fcc $Ni_{0.82}Fe_{0.18}$ powder sample (JCPDS:04-003-2245), while the peaks marked with an asterisk and triangle-down come from the copper and its contamination, respectively.

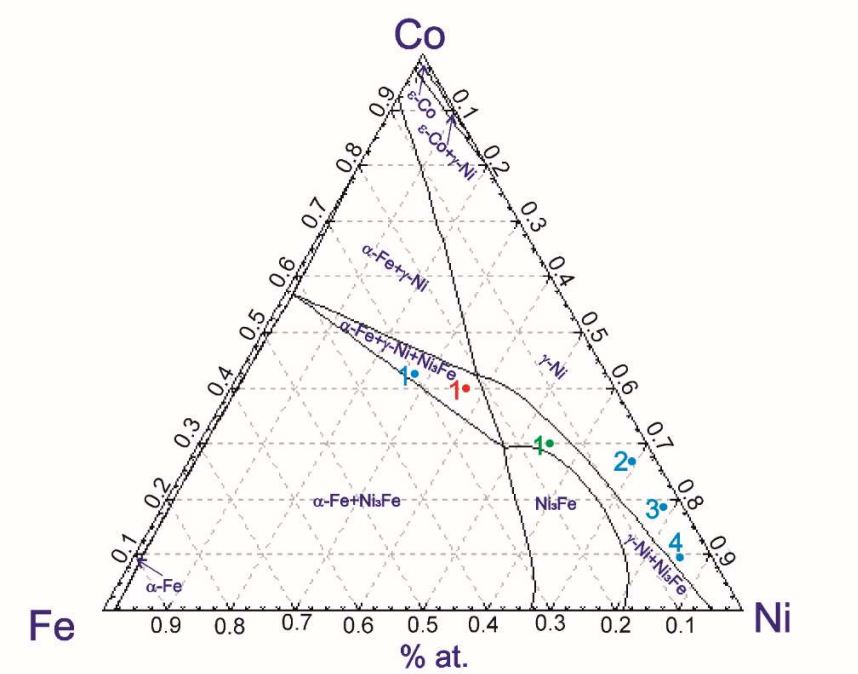

Figure 12. Ternary phase diagram of the FeCoNi system – isothermal cross-section at 293 K generated using the FactStage package and the SGTE database with points indicating the chemical composition of the samples (blue points – 100 nm diameter NWs, red point – 30 nm diameter NWs and green point – flat sample). The number from 1 to 4 correspond to the cathodic potentials from -1.0 V to -1.8 V.

Table 2. Results of XRD measurements of 100 nm diameter nanowires with lattice parameter (a), and average crystallite size (D).

2θ [deg]					
hkl	Reference*	-1.0 V	-1.2 V	-1.4 V	-1.8 V
111	44.23	43.95	44.15	44.30	44.37
200	51.53	51.21	51.44	51.62	51.75
220	75.87	75.6	75.76	75.95	76.08
311	92.25	91.78	92.16	92.51	92.71
222	97.69	97.32	97.57	97.85	98.08
Relative intensity [%]					
hkl	Reference*	-1.0 V	-1.2 V	-1.4 V	-1.8 V
111	100	100	100	100	100
200	41.8	17.5	12.0	21.6	20.8
220	16.4	8.2	6.4	30.4	25.8
311	14.6	4.2	4.6	9.8	6.9
222	4.0	2	2	2.9	2.4
a [Å]	3.544	3.565	3.555	3.538	3.530
D [nm]	-	12	18	19	22

* *the fcc $Ni_{0.82}Fe_{0.18}$ powder sample (JCPDS:04-003-2245)*

The increasing cathodic potential and the associated increase in the Ni content caused the changes in the peak positions. The shifts of the (111) and (220) peaks in nanowires with a diameter of 100 nm are shown in Figure 13. Peak maxima moves towards higher angular values as the cathodic current increases. Such a shift is caused by the modification of the atomic distance due to the replacement of Fe and Co atoms with Ni atoms, which results from the changes in the chemical composition. As Ni content increases, the Fe and Co content decrease, which taking into account that the Fe (1.72 Å) and Co (1.67 Å) atomic radii are larger than the radius of the Ni (1.62 Å) may be responsible for shortening the lattice parameter. Moreover, as can be seen from the calculated lattice parameters (Table 2), with the increase in the nickel content this parameter approaches to the Ni lattice constant (a_{Ni} = 3.52 Å in the fcc structure). Similarly, Dalavi *et al.* observed expansion of the lattice with an increase in Fe content in FeCoNi monocrystalline alloys [83]. The changes in the lattice parameter caused by modification of the chemical composition were also observed in FeCoNi films [74], [88].

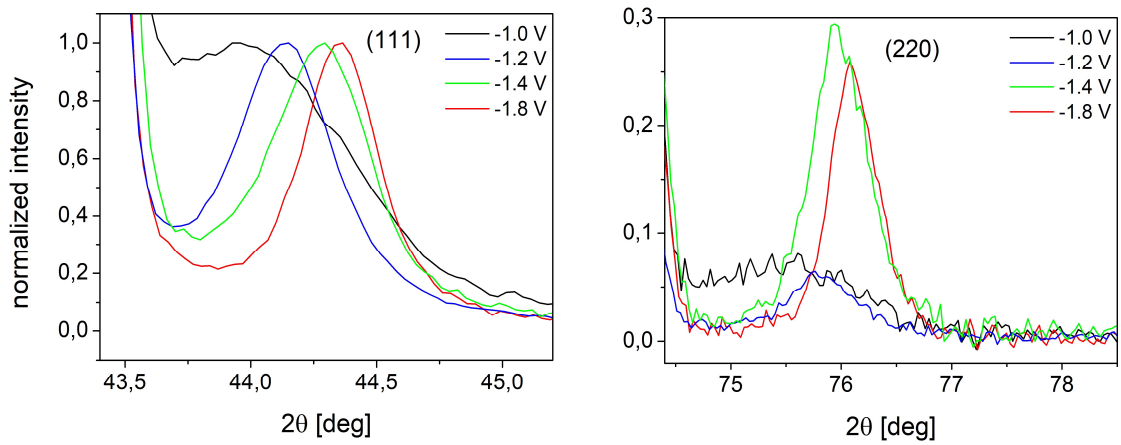

Figure 13. The (111) and (220) peaks with a visible shift towards higher 2Θ values with increasing cathodic potential (measured for 100 nm diameter nanowires).

Besides, the shift in the peak positions, a narrowing of the XRD reflection was observed. The normalized (220) peaks are shown in the inset of Figure 14. As can be seen, the width of the peaks decreases with increasing cathodic voltage (Ni content increases and the Co and Fe decrease), which suggests an increase in crystallite size for higher voltages. Calculations based on the Scherrer equation, shown in Figure 14, confirmed these observations. The average size of the crystallites, estimated with an error of 1 nm (larger only in the case of the smallest potential due to the inaccuracy of FWHM (full width at half maximum) determination), ranged from 12 to 22 nm for the lowest and highest voltage, respectively. The change in crystallite size with increasing voltage can be related to the change in current density. Higher current density at more cathodic potentials creates favorable conditions for crystal growth without ion deficiency, which promotes large crystallite sizes. Moreover, a greater amount of Ni that crystallizes in its own structure with a low content of Fe and Co, which can be treated as impurities in the Ni lattice, may also explain the observed increase in crystal size. A decrease in the grain size with increasing Co content was also observed by Long *et al.* in FeCoNi coatings [86] and Yanai *et al.* in FeCoNi films [85].

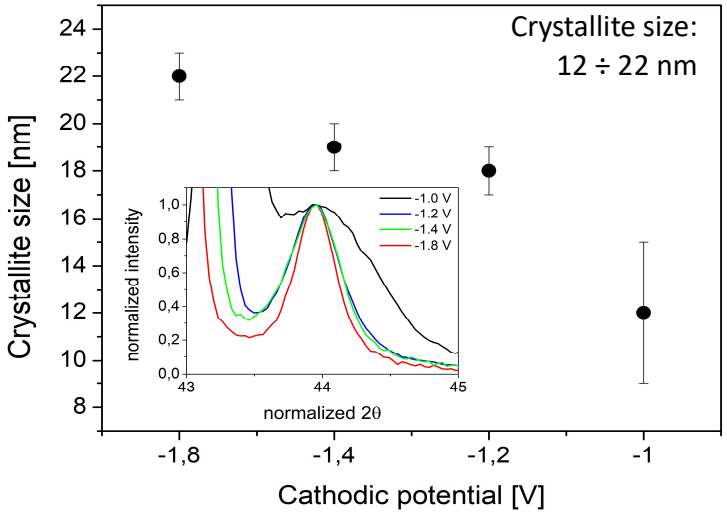

Figure 14. The mean value of crystallite size calculated according to the Scherrer formula based on the (220) peak broadening (measured for 100 nm diameter nanowires).

XRD measurements were also performed for nanowires with a diameter of 30 nm (Fig. 15a). These nanowires were deposited in the membranes covered with a gold layer, which shows the most intense peak in the same position as the (111) FeCoNi reflex. The first pattern measured for a pure gold-coated membrane indicates the peaks characteristic of gold. Subsequent patterns, apart from gold reflections (unmarked), reveal low-intensity peaks described by Miller indices (blues), assigned to the fcc phase of FeCoNi. The most intense (111) peak coming from FeCoNi is observed at 44.4°, which is also the position of the (200) reflex coming from gold. The increasing intensity of these peaks may suggest an increasing contribution of FeCoNi peaks (Fig. 15b). This can be attributed to a better filling degree (increase in total charge, Fig. 3 insets) and more distinct texture along the (111) direction (Fig.10b). Moreover, the shift in peak positions towards higher angles with more cathodic potential shows the same changes as observed in 100 nm diameter nanowires, indicating a shortening of the lattice parameters. The shift also confirms that this peak is a superposition of the reflexes coming from the FeCoNi alloy and gold. Additionally, the patterns measured for the samples prepared at low and medium potentials show well-distinguished (220) peaks and low-intensity (200) and (311) peaks. Furthermore, in the case of the nanowires deposited at -1.2 V, two peaks arise, which can be assigned to the hcp Ni-based alloy. Such a mixture of hcp and fcc structure has also been observed in FeCoNi nanowires with a similar chemical composition [87] and in films with high Co content (61 at%) [86]. Besides this small hcp fraction, the above results show a similar structural composition, which will not be analyzed in detail due to the mentioned superposition and low-intensity peaks. The very low peak intensities are due to the small amount of material which, in the case of membranes with a pore diameter of 30 nm, is embedded in pores constituting only 0.14% of the sample surface.

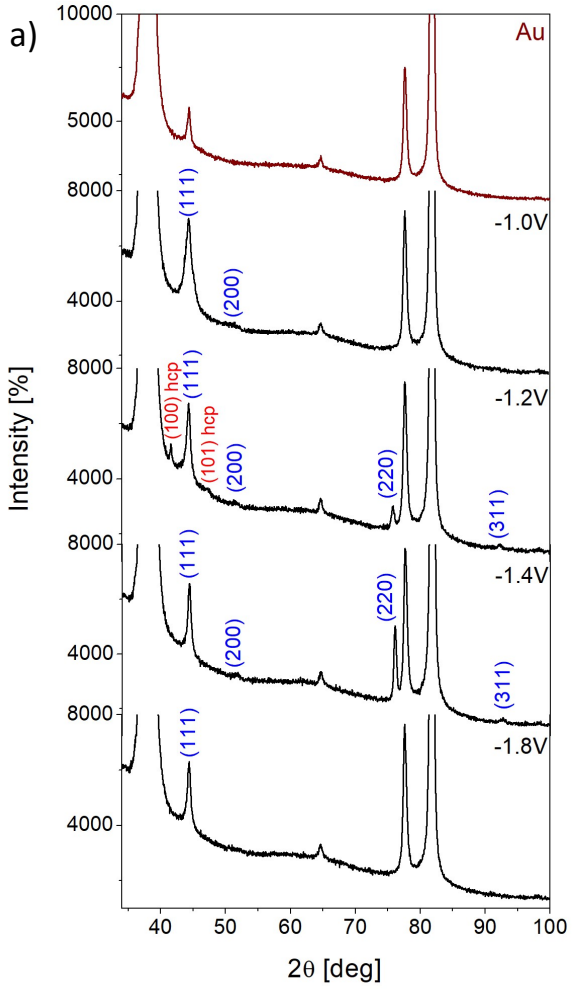

Figure 15. X-ray diffraction patterns measured for the FeCoNi nanowires with a diameter of 30 nm embedded in the polycarbonate membranes (a) and superposition of (111) and (200) peaks coming from FeCoNi NWs and Au gold layer (b), respectively. The assigned peaks correspond to the fcc FeCoNi (blue description; JCPDS:04-003-2245) and hcp FeCoNi (red description; AtomWork calculator). Non described peaks come from gold.

The preferred growth direction indicated by XRD measurements is consistent with the information taken from high-resolution TEM analysis. The performed studies reveal that for both nanowire diameters, the samples show a texture along the [111] direction or the [220] direction depending on the applied cathodic potential.

Magnetic properties

The magnetic measurements of the FeCoNi nanowires were performed at room temperature with the magnetic field applied along the nanowire axis and perpendicular to it. The hysteresis loops of the FeCoNi with diameters of 30 nm and 100 nm deposited at the different potentials are presented in Fig. 16. Pronounced magnetic anisotropy with an easy axis along nanowires was observed for all nanowires, regardless of diameter and composition.

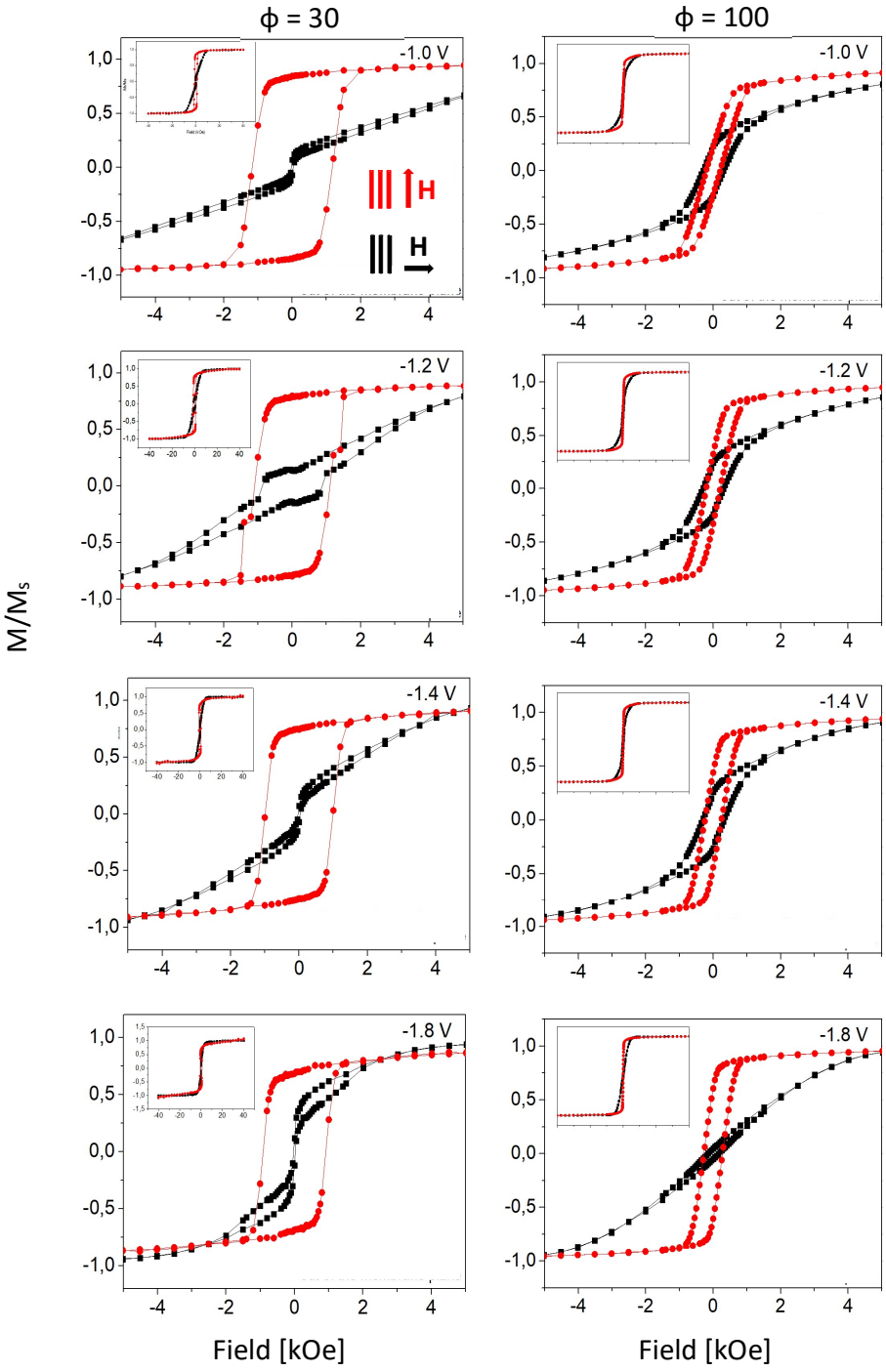

Figure 16. Hysteresis loops measured at room temperature with a magnetic field applied in the membrane plane and out of the membrane plane for nanowires with a diameter of 30 nm (ϕ = 30 nm) and 100 nm (ϕ = 100 nm) deposited at different cathodic potentials (specified in the respective figures). The magnetization (M) value was normalized to the saturation magnetization (M_s).

The magnetic behavior of nanowires is determined by completion between magnetocrystalline anisotropy, shape anisotropy, magnetoelastic anisotropy and dipolar interactions [16], [46], [51], [75], [89]. Magnetocrystalline anisotropy may contribute to effective anisotropy only in single crystalline samples or in samples with clearly visible texture. Polycrystalline samples without a preferred orientation of grains do not possess magnetocrystalline anisotropy [90]. The easy axis in fcc FeCoNi alloys lies along [111] direction [91], which is typical for a Ni-based fcc alloy. The shape anisotropy in high aspect ratio nanowires induces an easy axis along nanowire axis and is larger than the magnetocrystalline anisotropy in Fe, Ni and Co (fcc) [40], [92]–[96]. The magnetoelastic anisotropy, arising due to stresses between the template and the nanowires, can be neglected at room temperature because its value is much smaller than the shape anisotropy [94], [97]. The last contribution connected with dipolar interaction, if appears, will cause an alignment of the easy axis perpendicular to the nanowire axis.

The nanowires with a diameter of 30 nm showed more rectangular hysteresis measured with a magnetic field applied along nanowires and significantly greater values of coercivity and squareness. Changes in the hysteresis loop shapes for nanowires with different diameters are known in the literature and results from smaller inter-wire interactions as the packing factor decreases (porosity) [48], [98]. Furthermore, the nanowires with diameters smaller than 55 nm are expected to be single-domain wires [98], which changes the magnetization reversal process. Structural studies (XRD/TEM) indicate [111] growth direction or the [220] texture at lower and higher potentials, respectively. In nanowires with texture along the [111] direction, magnetocrystalline and shape anisotropies act in the same direction, increasing effective anisotropy along the nanowire axis. Moreover, for 30 nm diameter NWs, the low porosity templates suggest non-interacting nanowires with negligible dipolar interactions, which additionally increase coercivity and squareness. On the other hand, the texture along [220] deviates from the easy axis direction by about 35^{o}, thus it slightly contributes to the anisotropy along the nanowires axis. However, in the case of nanowires with a diameter of 100 nm, stronger dipole interactions, associated with the relatively small inter-wire distance, give the contribution to the magnetization alignment in the direction perpendicular to the nanowire axis and overshadow the effect of both anisotropy contributions.

The values of saturation magnetization (M_S), coercivity (H_c) and squareness (M_R/M_s) measured with a magnetic field applied along nanowires are presented in Fig. 17. The saturation magnetization normalized to the membrane surface (Fig. 17a) decreases with increasing electrodeposition rate (cathodic potential increases). This behavior is consistent with the decrease in the charge reduced at the cathode, assigned to the decreasing filling degree. The smaller amount of magnetic material embedded into the membrane is one of the reasons for the observed magnetization saturation drop. The second reason may be changes in the chemical composition. Samples with higher M_S values contain a smaller amount of Ni (Fig. 18a-b), which has three and four times lower saturation magnetization (M_S(Ni) = 57.5 emu/g) than cobalt (162.7 emu/g) and iron (217.9 emu/g), respectively [79], [84], [99]. The described M_S variation as a function of applied potential was observed for both 30 nm and 100 nm diameter nanowires, but at the lowest potential, the amount of Ni was significantly smaller in the nanowires with a diameter of 100 nm, which may explain the large increase in saturation magnetization for this sample (Fig. 18a-b). There is also a significant difference in the M_S values measured for nanowires with diameters of 30 nm and 100 nm deposited at other potentials, which is related to the much higher porosity of membranes with a pore diameter of 100 nm equaled to 3.1 % compared to 0.14 % for membranes with a pore size of 30 nm [57].

Higher pore density means a greater amount of magnetic material contributing to the saturation magnetization.

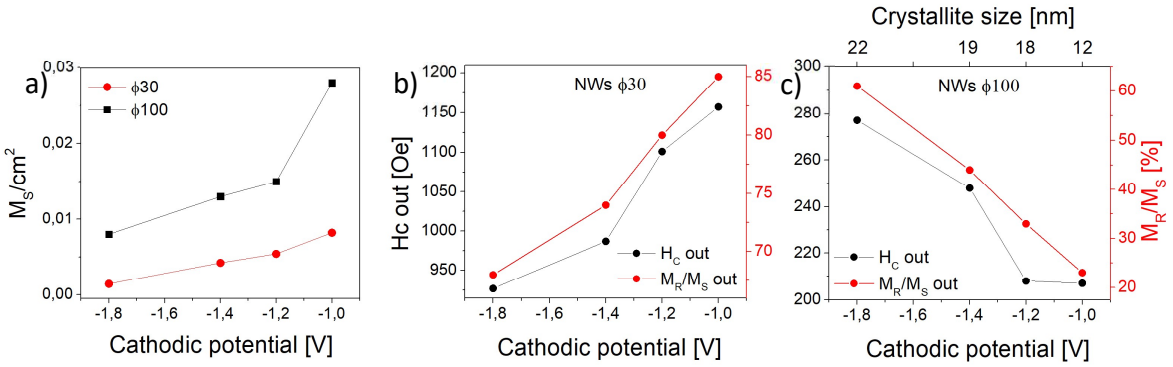

Figure 17. Saturation magnetization (a), out of plane coercivity and squareness (b, c) shown as a function of cathodic voltage (and crystallite size) for nanowires with diameters of 30 nm and 100 nm.

A surprising behavior was observed for coercivity and squareness dependence on the applied cathodic potential (Fig. 17 b-c). Both of these values demonstrate extremely different dependencies on the nanowire diameters. In the case of nanowires with a diameter of 100 nm, the expected increase in coercivity and squareness was observed with increasing cathodic voltage. This can be explained by the faster deposition rate, which resulted in a lower filling degree and therefore a more porous structure with a larger number of defects. These defects can block the domain wall movement and lead to a coercivity increase [51], [52]. Changes in the squareness, but also coercivity, can be attributed to smaller dipolar interactions caused by reduced saturation magnetization. Theoretically predicted and experimentally observed narrower, less squared and more oblique-shaped hysteresis has been reported for nanowires with decreasing distance thus increasing dipolar interactions [47]–[49], [54]–[56]. For nanowires with a diameter of 100 nm, the coercivity and squareness increased with increasing Ni content and decreasing Co and Fe content (Fig. 18b-c). These chemical changes resulted in a smaller saturation magnetization, which caused weaker magnetostatic interactions leading to higher coercivity and squareness. Together with the Ni content increase, an expansion of the grain size was observed (Fig. 17c). In our case, the larger the grains, the higher values of the coercivity and squareness were noticed. It is usually assumed that the grain boundary can hinder the domain wall movement, thus the larger the crystallite size, the lower the grain boundary density occurs, which should cause the lowering of the coercivity [52], [85], [100]. The observed discrepancy can again be attributed to the dipolar interactions, which in nanowires with a diameter of 100 nm, turned out to be the dominant factor determining coercivity and squareness. Therefore, the higher the saturation magnetization, the higher the dipolar interactions and the smaller the coercivity and squareness [42].

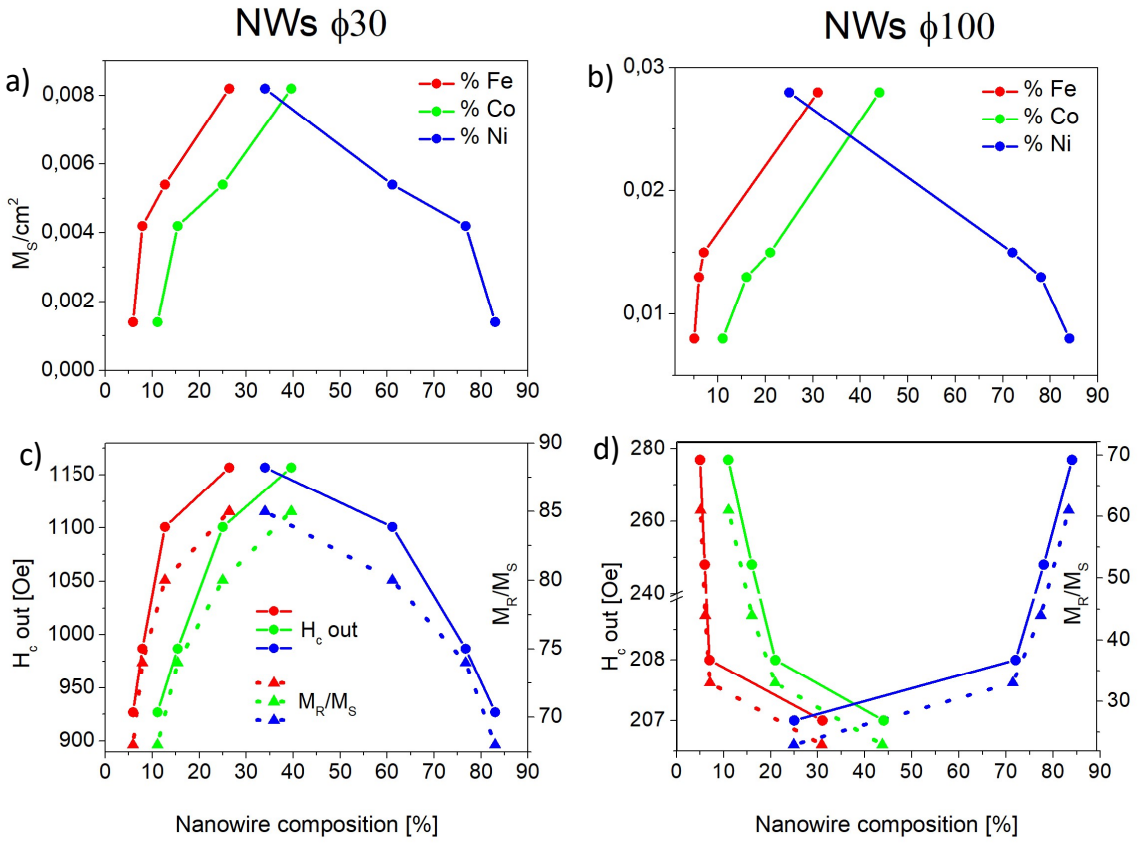

Figure 18. Saturation magnetization, out of plane coercivity and squareness shown as a function of Fe, Co and Ni content for nanowires with diameters of 30 nm (a, c) and 100 nm (b, d).

Unexpected changes in coercivity and squareness were noted for nanowires with a diameter of 30 nm (Fig. 17b). In this case, both values decrease with increasing cathodic voltage. Nanowires with a diameter of 30 nm, like nanowires with a diameter of 100 nm, show the same changes in the chemical composition with an increase in Ni content and decreasing total charge reduced at the cathode as a function of cathodic potential. There are also the same trends in the growth rates. Despite these similarities, there is an important differentiating factor, which is porosity, as mentioned above. In nanowires with a diameter of 30 nm, which show low porosity, very weak dipolar interactions do not reduce coercivity and squareness, therefore these parameters are much higher than in nanowires with larger diameters.

Thus, in the case of non-interacting nanowires, the coercivity and squareness behave as saturation magnetization, i.e. they increase with increasing Fe and Co content (Fig. 18c). An increase in coercivity with increasing Co content has also been observed in the literature [29], [47], [77], [101]. According to Shama *et al.*, for weak magnetostatic interactions between nanowires – as in the case of nanowires with a diameter of 30 nm – an increase in Ni content results in a decrease in the saturation magnetization and coercivity [79]. Changes in coercivity and squareness as a function of chemical composition can be analyzed based on the magnetic parameters of Fe, Co and Ni nanowires. A larger amount of Fe and/or Co,

showing higher values of saturation magnetization, coercivity and squareness, directly results in an increase in these values in FeCoNi nanowires [86], [101]. At the same time, the opposite behavior observed in nanowires with a diameter of 100 nm results from dipolar interactions, which increased when the amount of elements with high saturation magnetization and coercivity increased.

Dipolar interactions increase strongly with increasing nanowire length [39], [42], [46]. Studies on the influence of the geometrical parameters of FeCoNi nanowires on the magnetic properties (paper in preparation) showed a significant increase in coercivity and squareness as nanowire length drops down to 1.5 µm. This suggests that dipolar interactions can be also neglected in nanowires with a diameter of 100 nm, which indicates that both 30 nm and 100 nm nanowires can be considered as potential candidates for race track memory applications.

Conclusions

FeCoNi nanowires deposited at different cathodic potentials showed clear changes in their chemical composition, which resulted in the desired modification of the magnetic properties. As the cathodic voltage increased, the Ni content increased, while the concentration of Fe and Co decreased. Regardless of chemical composition, the nanowires crystalized in the fcc structure with a small fraction of the hcp phase appearing in one 30 nm diameter sample. The samples showed preferred growth along the [111] or [220] directions. The lattice parameter decreased, while the crystallite size expanded with an increasing cathodic potential. Depending on the nanowire diameter, a decrease or increase in the coercivity and squareness were observed with increasing voltage for samples with a diameter of 30 nm and 100 nm, respectively. Such an opposite behavior was explained by the dominant role of the magnetostatic interaction in nanowires with a diameter of 100 nm. Nanowires of both diameters seem to be promising candidates for racetrack memory applications.

Acknowledgment

This research was supported by a French Government Scholarship.

Conflict of Interest

The authors declare that they have no conflict of interest.

References

[1] A. Salati, A. Ramazani, and M. Almasi Kashi, Tuning hyperthermia properties of FeNiCo ternary alloy nanoparticles by morphological and magnetic characteristics, *J. Magn. Magn. Mater.*, 2020, 498, 166172, doi: 10.1016/j.jmmm.2019.166172.

[2] A. Mukhtar, B. S. Khan, and T. Mehmood, A study of growth mechanism of Fe nanowires and nanotube via template-based electrodeposition, *Int. J. Electrochem. Sci.*, 2017, 12, 4574–4584, doi: 10.20964/2017.05.82.

[3] J. A. Moreno, C. Bran, M. Vazquez, and J. Kosel, Cylindrical Magnetic Nanowires Applications, *IEEE Trans. Magn.*, 2021, 57, 1–17, doi: 10.1109/tmag.2021.3055338.

[4] A. Salati, A. Ramazani, and M. Almasi Kashi, Tuning hyperthermia properties of FeNiCo ternary alloy nanoparticles by morphological and magnetic characteristics, *J. Magn. Magn. Mater.*, 2020, 498, 166172, doi: 10.1016/j.jmmm.2019.166172.

[5] X. Kou, X. Fan, R. K. Dumas, Q. Lu, Y. Zhang, H. Zhu, X. Zhang, K. Liu, J. Q. Xiao, Memory effect in magnetic nanowire arrays, *Adv. Mater.*, 2011, 23, 1393–1397, doi:10.1002/adma.201003749.

[6] G. Yang, J. Tang, S. Kato, Q. Zhang, L. C. Qin, M. Woodson, J. Liu, J. W. Kim, P. T. Littlehei, C. Park, O. Zhou, Magnetic nanowire based high resolution magnetic force microscope probes, *Appl. Phys. Lett.*, 2005, 87, 1–3, doi: 10.1063/1.2043237.

[7] D. Li, H. Liu, and L. Feng, A Review on Advanced FeNi-Based Catalysts for Water Splitting Reaction, *Energy and Fuels*, 2020, 34, 13491–13522, doi: 10.1021/acs.energyfuels.0c03084.

[8] X. Z. Xiang, W. Y. Gong, M. S. Kuang, and L. Wang, Progress in application and preparation of silver nanowires, *Rare Met.*, 2016, 35, 289–298, doi: 10.1007/s12598-016-0695-6.

[9] J. Pablo-Navarro, S. Sangiao, C. Magén, and J. M. de Teresa, Magnetic Functionalization of Scanning Probes by Focused Electron Beam Induced Deposition Technology, *Magnetochemistry*, 2021, 7, 140, doi: 10.3390/magnetochemistry7100140.

[10] X. Xu, R. Wang, P. Nie, Y. Cheng, X. Lu, L. Shi and J. Sun, Copper Nanowire-Based Aerogel with Tunable Pore Structure and Its Application as Flexible Pressure Sensor, *ACS Appl. Mater. Interfaces*, 2017, 9, 14273–14280, doi: 10.1021/acsami.7b02087.

[11] Y. Mashraei, S. Amara, Z. Albu, Y. P. Ivanov, and J. Kosel, Ultra-Low Power Corrosion Sensor Made of Iron Nanowires on Magnetic Tunnel Junctions, *Adv. Eng. Mater.*, 2018, 20, 1–6, doi: 10.1002/adem.201800337.

[12] P. C. Pinheiro, D. S. Tavares, A. L. Daniel-da-Silva, C. B. Lopes, E. Pereira, J. P. Araujo, C. T. Sousa and T. Trindade, Ferromagnetic sorbents based on nickel nanowires for efficient uptake of mercury from water, *ACS Appl. Mater. Interfaces*, 2014, 6, pp. 8274–8280, doi: 10.1021/am5010865.

[13] J. Um, M. R. Z. Kouhpanji, S. Liu, Z. N. Porshokouh, S. Y. Sung, J. Kosel and B. Stadler, Fabrication of Long-Range Ordered Aluminum Oxide and Fe/Au Multilayered Nanowires for 3-D Magnetic Memory, *IEEE Trans. Magn.*, 2020, 56, 2–7, doi: 10.1109/TMAG.2019.2942946.

[14] Y. P. Ivanov, A. Chuvilin, S. Lopatin, and J. Kosel, Modulated Magnetic Nanowires for Controlling Domain Wall Motion: Toward 3D Magnetic Memories, *ACS Nano*, 2016, 10, 5326–5332, doi: 10.1021/acsnano.6b01337.

[15] S. Bochmann, D. Döhler, B. Trapp, M. Staňo, O. Fruchart, and J. Bachmann, Preparation and physical properties of soft magnetic nickel-cobalt three-segmented nanowires, *J. Appl. Phys.*, 2018, 124, 163907-10 doi: 10.1063/1.5049892.

[16] C. Bran, J. A. Fernandez-Roldan, R. P. Del Real, A. Asenjo, O. Chubykalo-Fesenko, and M. Vazquez, Magnetic configurations in modulated cylindrical nanowires, *Nanomaterials*, 2021, 11, 1–27, doi: 10.3390/nano11030600.

[17] S. Parkin and S. H. Yang, Memory on the racetrack *Nat. Nanotechnol.*, 2015, 10, 195–198, doi: 10.1038/nnano.2015.41.

[18] S. Bochmann, A. Fernandez-Pachecob, M. Mačkovićc, A. Neffd, K. R. Siefermannd, E. Spieckerc, R. P. Cowburnb and J. Bachmann, Systematic tuning of segmented magnetic nanowires into three-dimensional arrays of 'bits' *RSC Adv.*, 2017, 7, 37627–37635, doi: 10.1039/c7ra06734h.

[19] D. Chiba, G. Yamada, T. Koyama, K. Ueda, H. Tanigawa, S. Fukami, T. Suzuki, N. Ohshima, N.

Ishiwata, Y. Nakatani and T. Ono, Control of Multiple Magnetic Domain Walls by Current in a Co/Ni Nano-Wire, *Appl. Phys. Express*, 2010, vol. 3, pp. 073004-3, doi: 10.1143/APEX.3.073004.

[20] S. S. P. Parkin, M. Hayashi, and L. Thomas, Magnetic Domain-Wall Racetrack Memory, *Science*, 2008, 320, 190–194, doi: 10.1126/science.1145799.

[21] E. C. Burks, D. A. Gilbert, P. D. Murray, C. Flores, T. E. Felter, S. Charnvanichborikarn, S. O. Kucheyev, J. D. Colvin, G. Yin, and K. Liu, 3D Nanomagnetism in Low Density Interconnected Nanowire Networks, *Nano Lett.*, 2021, 21, 716–722, doi: 10.1021/acs.nanolett.0c04366.

[22] A. S. Samardak, E. V. Sukovatitsina, A. V. Ognev, L. A. Chebotkevich, R. Mahmoodi, S. M. Peighambari, M. G. Hosseini, F. Nasirpouri, High-density nickel nanowire arrays for data storage applications, *J. Phys. Conf. Ser.*, 2012, 345, 012011-5, doi: 10.1088/1742-6596/345/1/012011.

[23] T. da Câmara Santa Clara Gomes, N. Marchal, F. Abreu Araujo, Y. Velázquez Galván, J. de la Torre Medina, and L. Piraux, Magneto-transport in flexible 3D networks made of interconnected magnetic nanowires and nanotubes, *Nanomaterials*, 2021, 11, 1–19, doi: 10.3390/nano11010221.

[24] N. Mansouri, N. Benbrahim-Cheriefa, E. Chainetb, F. Charlotc, T. Encinasc, S. Boudinara, B. Benfeddaa, L. Hamadoua and A. Kadri, Electrodeposition of equiatomic FeNi and FeCo nanowires: Structural and magnetic properties, *J. Magn. Magn. Mater.*, 2019, 493, 165746, doi: 10.1016/j.jmmm.2019.165746.

[25] S. Agramunt-Puig, N. Del-Valle, E. Pellicer, J. Zhang, J. Nogués, C. Navau, A. Sanchez, and J. Sort, Modeling the collective magnetic behavior of highly-packed arrays of multi-segmented nanowires, *New J. Phys.*, 2016, 18, 013026-8, doi: 10.1088/1367-2630/18/1/013026.

[26] F. Nasirpouri, Template electrodeposition of magnetic nanowire arrays, *Transworld Research Network*, 2007, 37, 661, ISBN: 978-81-7895-304-5.

[27] X. Geng and E. J. Podlaha, Coupled, Simultaneous Displacement and Dealloying Reactions into Fe-Ni-Co Nanowires for Thinning Nanowire Segments, *Nano Lett.*, 2016, 16, 7439–7445, doi: 10.1021/acs.nanolett.6b03065.

[28] Y. Xiao, Q. Xu, J. Zhang, X. Yin, and S. Duan, Preparation and Magnetic Properties of Fe-Co–Ni Magnetic Nanowire Arrays with Three-Dimensional Periodic Structures, *J. Supercond. Nov. Magn.*, 2023, 36, 1161–1170, doi: 10.1007/s10948-023-06555-y.

[29] S. Budi, S. Muhab, A. Purwanto, B. Kurniawan, and A. Manaf, Effect of the electrodeposition potential on the magnetic properties of FeCoNi films, *Mater. Sci. Pol.*, 2019, 37, 389-394, doi: 10.2478/msp-2019-0044.

[30] X. Liu, G. Zangari, and M. Shamsuzzoha, Structural and Magnetic Characterization of Electrodeposited, High Moment FeCoNi Films, *J. Electrochem. Soc.*,2003, 150, C159, doi: 10.1149/1.1545462.

[31] H. Hu, M. Tan, and L. Liu, Anomalous codeposition mechanism of Co-Ni alloy nanowires, *J. Alloys Compd.*, 2017, 715, 384–389, doi: 10.1016/j.jallcom.2017.05.002.

[32] A. Bai, C. C. Hu, and T. C. Wen, Composition control of ternary Fe-Co-Ni deposits using cyclic voltammetry, *Electrochim. Acta*, 2003, 48, 2425–2434, doi: 10.1016/S0013-4686(03)00266-4.

[33] O. Dragos, H. Chiriac, N. Lupu, M. Grigoras, and I. Tabakovic, Anomalous Codeposition of fcc NiFe Nanowires with 5–55% Fe and Their Morphology, Crystal Structure and Magnetic Properties, *J.*

Electrochem. Soc., 2016, 163, D83–D94, doi: 10.1149/2.0771603jes.

[34] C.-C. Hu and A. Bai, The Inhibition of Anomalous Codeposition of Iron-Group Alloys Using Cyclic Voltammetry, *J. Electrochem. Soc.*, 2002, 149, C615, doi: 10.1149/1.1511753.

[35] A. Saedi and M. Ghorbani, Electrodeposition of Ni-Fe-Co alloy nanowire in modified AAO template, *Mater. Chem. Phys.*, 2004, 91, 417–423, doi: 10.1016/j.matchemphys.2004.12.001.

[36] N. H. Phan, M. Schwartz, and K. Nobe, Electrodeposition of Fe-Ni-Co alloys part I: Direct current deposition, *J. Appl. Electrochem.*, 1991, 21, 672–677, doi: 10.1007/BF01034044.

[37] J. Gong, S. Riemer, A. Morrone, V. Venkatasamy, M. Kautzky, and I. Tabakovic, Composition Gradients and Magnetic Properties of 5–100 nm Thin CoNiFe Films Obtained by Electrodeposition, *J. Electrochem. Soc.*, 2012, 159, D447–D454, doi: 10.1149/2.082207jes.

[38] R. S. Larson, The Role of Homogeneous Chemical Kinetics in the Anomalous Codeposition of Binary Alloys, *J. Electrochem. Soc.*, 2007, 154, D427, doi: 10.1149/1.2747325.

[39] M. Kac, , A. Zarzycki, S. Kac, M. Kopec, M. Perzanowski, E. M. Dutkiewicz, K. Suchanek, A. Maximenko and M. Marszałek, Effect of the template-assisted electrodeposition parameters on the structure and magnetic properties of Co nanowire arrays, *Mater. Sci. Eng. B Solid-State Mater. Adv. Technol.*, 2016, 211, 75–84, doi: 10.1016/j.mseb.2016.06.004.

[40] I. Dobosz, W. Gumowska, and M. Czapkiewicz, Structure and magnetic properties of Co nanowires electrodeposited into the pores of anodic alumina membranes, *J. Solid State Electrochem.*, 2014, 18, 2963–2972, doi: 10.1007/s10008-014-2552-6.

[41] A. H. A. Elmekawy, E. Iashina, I. Dubitskiy, S. Sotnichuk, I. Bozhev, D. Kozlov, K. Napolskii, D. Menze and A. Mistonov, Magnetic properties of ordered arrays of iron nanowires: The impact of the length, *J. Magn. Magn. Mater.*, 2020, 532, 167951, doi: 10.1016/j.jmmm.2021.167951.

[42] S. Samanifar, M. Almasi Kashi, A. Ramazani, and M. Alikhani, Reversal modes in FeCoNi nanowire arrays: Correlation between magnetostatic interactions and nanowires length, *J. Magn. Magn. Mater.*, 2015, 378, 73–83, doi: 10.1016/j.jmmm.2014.10.155.

[43] G. C. Han, B. Y. Zong, and Y. H. Wu, Magnetic properties of magnetic nano-wire arrays, *INTERMAG Eur. 2002 - IEEE Int. Magn. Conf.*, 2002, 38, 2562–2564, doi: 10.1109/INTMAG.2002.1001219.

[44] G. C. Han, B. Y. Zong, P. Luo, and Y. H. Wu, Angular dependence of the coercivity and remanence of ferromagnetic nanowire arrays, *J. Appl. Phys.*, 2003, 93, 9202–9207, doi: 10.1063/1.1572197.

[45] F. Zighem, T. Maurer, F. Ott, and G. Chaboussant, Dipolar interactions in arrays of ferromagnetic nanowires: A micromagnetic study, *J. Appl. Phys.*, 2011, 109, 013910-8, doi: 10.1063/1.3518498.

[46] J. Wang, X. Hua, Y. Lia, H. Wena, Z. Zuoa, W.A. Muhammadb, J. Q. Xiaob and J Hu, Shape-dependent magnetic properties of gradient-diameter Co nanowire arrays, *J. Magn. Magn. Mater.*, 2018, 475, 502–507, doi: 10.1016/j.jmmm.2018.11.103.

[47] G. Kartopu, O. Yaļin, M. Es-Souni, and A. C. Başaran, Magnetization behavior of ordered and high density Co nanowire arrays with varying aspect ratio, *J. Appl. Phys.*, 2008, 103, 093915-12 doi: 10.1063/1.2917191.

[48] I. S. Dubitskiy, A. H. A. Elmekawy, E. G. Iashina, S. V. Sotnichuk, K. S. Napolskii, D. Menzel and A. A. Mistonov, Effect of Interactions and Non-uniform Magnetic States on the Magnetization Reversal

of Iron Nanowire Arrays, *J. Supercond. Nov. Magn.*, 2021, 34, 539–549, doi: 10.1007/s10948-020-05711-y.

[49] O. Pastukh, M. Kac, S. Pastukh, M. Krawczyk and Łukasz Laskowski, Magnetic Behavior of the Arrays of Iron Cylindrical Nanostructures: Atomistic Spin Model Simulations, *Crystals*, 2023, 13, 1–16, doi: 10.3390/cryst13030537.

[50] A. Ramazani, M. Almasi Kashi, S. Ghanbari, and F. Eshaghi, Dual behaviors of magnetic Co xFe 1-x (0≤x≤1) nanowires embedded in nanoporous with different diameters, *J. Magn. Magn. Mater.*,2012, 324, 3193–3198, doi: 10.1016/j.jmmm.2012.05.036.

[51] H. Schlörb, V. Haehnel, M. S. Khatri, A. Srivastav, A. Kumar, L. Schultz and S. Fahler, Magnetic nanowires by electrodeposition within templates, *Phys. Status Solidi Basic Res.*, 2010, 247, 2364–2379, doi: 10.1002/pssb.201046189.

[52] M. Kac, A. Mis, B. Dubiel, K. Kowalski, A. Zarzycki, and I. Dobosz, Template-assisted iron nanowire formation at different electrolyte temperatures, *Materials (Basel).*, 2021, 14, 115732, doi: 10.3390/ma14154080.

[53] D. Li and E. J. Podlaha, Template-Assisted Electrodeposition of Porous Fe-Ni-Co Nanowires with Vigorous Hydrogen Evolution, *Nano Lett.*, 2019, 19, 3569–3574, doi:10.1021/acs.nanolett.9b00532.

[54] K. Nielsch, F. Müller, A. P. Li, and U. Gösele, Uniform nickel deposition into ordered alumina pores by pulsed electrodeposition, *Adv. Mater.*, 2000, 12, 582–586, doi: 10.1002/(SICI)1521-4095(200004)12:8<582::AID-ADMA582>3.0.CO;2-3.

[55] L. Sampaio, E. H. C. P. Sinnecker, G. Cernicchiaro, and M. Knobel, Magnetic microwires as macrospins in a long-range dipole-dipole interaction, *Phys. Rev. B - Condens. Matter Mater. Phys.*, 2000, 61, 8976–8983, doi: 10.1103/PhysRevB.61.8976.

[56] J. Velázquez, C. García, M. Vázquez, and A. Hernando, Interacting amorphous ferromagnetic wires: A complex system, *J. Appl. Phys.*, 1999, 85, 2768–2774, doi: 10.1063/1.369592.

[57] M. Kac, A. Zarzycki, S. Kac, M. Kopec, M. Perzanowski, E. M. Dutkiewicz, K. Suchanek, A. Maximenko and M. Marszałek, Effect of the template-assisted electrodeposition parameters on the structure and magnetic properties of Co nanowire arrays, *Mater. Sci. Eng. B Solid-State Mater. Adv. Technol.*, 2016, 211, 75–84, doi: 10.1016/j.mseb.2016.06.004.

[58] N. Zech, E. J. Podlaha, and D. Landolt, Anomalous Codeposition of Iron Group Metals: I. Experimental Results, *J. Electrochem. Soc.*, 1999, 146, 2886–2891, doi: 10.1149/1.1392024.

[59] D. Grujicic and B. Pesic, Iron nucleation mechanisms on vitreous carbon during electrodeposition from sulfate and chloride solutions, *Electrochim. Acta*, 2005, 50, 4405–4418, doi: 10.1016/j.electacta.2005.02.013.

[60] D. Grujicic and B. Pesic, Electrochemical and AFM study of cobalt nucleation mechanisms on glassy carbon from ammonium sulfate solutions, *Electrochim. Acta*,2004, 49, 4719–4732, doi: 10.1016/j.electacta.2004.05.028.

[61] D. Grujicic and B. Pesic, Electrochemical and AFM study of nickel nucleation mechanisms on vitreous carbon from ammonium sulfate solutions, *Electrochim. Acta*, 2006, 51, 2678–2690, doi: 10.1016/j.electacta.2005.08.017.

[62] G. Nemtoi, H. Chiriac, O. Dragos, M.-O. Apostu, and D. Lutic, The Voltammetric Characterization of the Electrodeposition of Cobalt , Nickel and Iron on Gold Disk Electrode, *Acta Chem. Iasi*, 2009, 17, 151–168, https://api.semanticscholar.org/CorpusID:53330914.

[63] L. H. Mendoza-Huizar and C. H. Rios-Reyes, Cobalt electrodeposition onto polycrystalline gold from ammoniacal solutions, *Cent. Eur. J. Chem.*, 2013, 11, 1381–1392, doi: 10.2478/s11532-013-0269-5.

[64] I. Hanafi, A. R. Daud, and S. Radiman, Cyclic voltammetric study of Co-Ni-Fe alloys electrodeposition in sulfate medium, *AIP Conf. Proc.*, 2013, 1571, 120–124, doi: 10.1063/1.4858640.

[65] A. Dolati, M. Sababi, E. Nouri, and M. Ghorbani, A study on the kinetic of the electrodeposited Co-Ni alloy thin films in sulfate solution, *Mater. Chem. Phys.*, 2007, 102, 118–124, doi: 10.1016/j.matchemphys.2006.07.009.

[66] H. Nakano, M. Matsuno, S. Oue, M. Yano, S. Kobayashi, and H. Fukushima, Mechanism of anomalous type electrodeposition of Fe-Ni alloys from sulfate solutions, *Nippon Kinzoku Gakkaishi/Journal Japan Inst. Met.*, 2005, 69, 548–554, doi: 10.2320/jinstmet.69.548.

[67] C. Fan and D. L. Piron, Study of anomalous nickel-cobalt electrodeposition with different electrolytes and current densities, *Electrochim. Acta*, 1996, 41, 1713–1719, doi: 10.1016/0013-4686(95)00488-2.

[68] C. Srivastava, S. K Ghosh, S. Rajak, A. K. Sahu, R. Tewari, V. Kain, G. K. Dey, Effect of pH on anomalous co-deposition and current efficiency during electrodeposition of Ni-Zn-P alloys, *Surf. Coatings Technol.*, 2017, 313, 8–16, doi: 10.1016/j.surfcoat.2017.01.043.

[69] M. Arefpour, M. A. Kashi, A. Ramazani, and A. H. Montazer, Electrochemical pore filling strategy for controlled growth of magnetic and metallic nanowire arrays with large area uniformity, *Nanotechnology*, 2016, 27, 275605-12, doi: 10.1088/0957-4484/27/27/275605.

[70] S. Shin, B. H. Kong, B. S. Kim, K. M. Kim, H. K. Cho, and H. H. Cho, Over 95 % of large-scale length uniformity in template-assisted electrodeposited nanowires by subzero-temperature electrodeposition, *Nanoscale Research Letters*, 2011, 6, 1–8., doi:10.1186/1556-276X-6-467.

[71] J. Azevedo, C. T. Sousa, J. Ventura, A. Apolinario, A. Mendes, and J. P. Araujo, Ultra-long Fe nanowires by pulsed electrodeposition with full filling of alumina templates Ultra-long Fe nanowires by pulsed electrodeposition with full fi lling of alumina templates, *Mater. Res. Express*, 2014, 1, 015028-16, doi: 10.1088/2053-1591/1/1/015028.

[72] K. S. Napolskii, I. V. Roslyakova, A. A. Eliseeva, D. I. Petukhova, A. V. Lukashina, S.F. Chenb, C.P. Liub, G. A. Tsirlina, Tuning the microstructure and functional properties of metal nanowire arrays via deposition potential, *Electrochim. Acta*, 2011, 56, 2378–2384, doi: 10.1016/j.electacta.2010.12.013.

[73] X. X. Fan, H. N. Hu, S. M. Zhou, M. Yang, J. Du, and Z. Shi, Abnormal temperature dependence of coercivity in cobalt nanowires, *Chinese Phys. Lett.*, 2012, 29, 077802-4, doi: 10.1088/0256-307X/29/7/077802.

[74] X. Liu, G. Zangari, and M. Shamsuzzoha, Structural and Magnetic Characterization of Electrodeposited, High Moment FeCoNi Films, *J. Electrochem. Soc.*, 2003, 150, C159, doi: 10.1149/1.1545462.

[75] X. Zhang, H. Zhang, T. Wu, Z. Li, Z. Zhang, and H. Sun, Comparative study in fabrication and magnetic properties of FeNi alloy nanowires and nanotubes, *J. Magn. Magn. Mater.*, 2013, 331, 162–167, 2013, doi: 10.1016/j.jmmm.2012.11.033.

[76] I. Hanafi, A. R. Daud, and S. Radiman, Potentiostatic electrodeposition of Co-Ni-Fe alloy particles thin film in a sulfate medium, *Port. Electrochim. Acta*, 2017, 35, 1–12, doi: 10.4152/pea.201701001.

[77] U. Sarac, M. Kaya, and M. C. Baykul, A Comparative Study on Microstructures, Magnetic Features and Morphologies of Ternary Fe–Co–Ni Alloy Thin Films Electrochemically Fabricated at Different Deposition Potentials, *J. Supercond. Nov. Magn.*, 2019, 32, 917–923, doi: 10.1007/s10948-018-4774-9.

[78] M. Kac, A. Nykiel, O. Pastukh, M. Kopec, A. Zarzycki, A. Maximenko, M. Parlinska-Wojtan, E.M. Dutkiewicz, A. Kopia, Materials Science & Engineering B The role of the addition of Cu in alloyed and multilayered Fe-based nanowires, *Mater. Sci. Eng. B*, 2022, 281, 115732, doi: 10.1016/j.mseb.2022.115732.

[79] G. Sharma and C. A. Grimes, Synthesis, characterization, and magnetic properties of FeCoNi ternary alloy nanowire arrays, *J. Mater. Res.*, 2004, 19, 3695–3703, doi: 10.1557/JMR.2004.0476.

[80] N. Mansouri, N. Benbrahim-Cheriefa, E. Chainetb, F. Charlotc, T. Encinasc, S. Boudinara, B. Benfeddaa, L. Hamadoua, A. Kadria, Electrodeposition of equiatomic FeNi and FeCo nanowires: Structural and magnetic properties, *J. Magn. Magn. Mater.*, 2019, 493, 165746, doi: 10.1016/j.jmmm.2019.165746.

[81] Piotr Ledwig, M. Kac, A. Kopia, J. Falkus and B. Dubiel, Microstructure and Properties of Electrodeposited Nanocrystalline Ni-Co-Fe Coatings, *Materials*, 2021, 14, 1–16, doi: 10.3390/ma 14143886.

[82] Y. Zhang and D. G. Ivey, Characterization of Co – Fe and Co – Fe – Ni soft magnetic films electrodeposited from citrate-stabilized sulfate baths, *Materials Science and Engineering B*, 2007, 140, 15–22, doi: 10.1016/j.mseb.2007.03.004.

[83] S. B. Dalavi, J. Theerthagiri, M. Manivel Raja, and R. N. Panda, Synthesis, characterization and magnetic properties of nanocrystalline FexNi80-xCo20 ternary alloys, *J. Magn. Magn. Mater.*, 2013, 344, 30–34, doi: 10.1016/j.jmmm.2013.05.026.

[84] C. Toparli, B. Ebin, and S. Gürmen, Synthesis, structural and magnetic characterization of soft magnetic nanocrystalline ternary FeNiCo particles, *J. Magn. Magn. Mater.*, 2017, 423, 133–139, doi: 10.1016/j.jmmm.2016.09.005.

[85] T. Yanai, K. Koda, J. Kaji, H. Aramaki, K. Eguchi, K. Takashima, M. Nakano, H. Fukunaga, Electroplated Fe-Co-Ni films prepared in ammonium-chloride-based plating baths, *AIP Adv.*, 2018, 8, 056127-5, doi: 10.1063/1.5007782.

[86] V. C. Long, U. Saraç, M. C. Baykul, L. D. Trong, Ş. Ţălu, and D. N. Trong, Electrochemical Deposition of Fe–Co–Ni Samples with Different Co Contents and Characterization of Their Microstructural and Magnetic Properties, *Coatings*, 2022, 12, 346-14, doi: 10.3390/coatings12030346.

[87] P. Fu, G. Chen, Y. Xu, P. Cai, and X. H. Wang, Electrodeposition and magnetic properties of ternary Fe-Co-Ni alloy nanowire arrays with high squareness ratio, *Mater. Sci. Pol.*, 2012, 30, 259–263, doi: 10.2478/s13536-012-0031-2.

[88] Y. Iwasaki, A. G. Kusne, and I. Takeuchi, Comparison of dissimilarity measures for cluster analysis of X-ray diffraction data from combinatorial libraries, *npj Comput. Mater.*, 2017, 3, 1-9, doi: 10.1038/s41524-017-0006-2.

[89] A. K. Srivastav and R. Shekhar, Crystal anisotropy induced temperature dependent magnetization in cobalt nanowires electrodeposited within alumina template, *J. Magn. Magn. Mater.*, 2014, 349, 21–26, doi: 10.1016/j.jmmm.2013.08.041.

[90] M. Getzlaff: *Fundamental of magnetism,* Angewandte Chemie International Edition, Germany, 2017, pp. 102.

[91] T. Okamoto, H. Yamada, S. Sugawara, S. Ishio, Magnetocrystalline Anisotropy of Single Crystals and Magnetic Properties of Evaporated Films in Co-Ni-Fe Ternary Alloy, *J. Magn. Soc. Jpn,* 1995, 19, 445-448 .

[92] A. Kumar, S. Fähler, H. Schlörb, K. Leistner, and L. Schultz, Competition between shape anisotropy and magnetoelastic anisotropy in Ni nanowires electrodeposited within alumina templates, *Phys. Rev. B - Condens. Matter Mater. Phys.*, 2006, 73, 1-5, doi: 10.1103/PhysRevB.73.064421.

[93] P. M. Paulus, F. Luis, M. Kröll, G. Schmid, and L. J. De Jongh, Low-temperature study of the magnetization reversal and magnetic anisotropy of Fe, Ni, and Co nanowires, *J. Magn. Magn. Mater.*, 2001, 224, 180–196, doi: 10.1016/S0304-8853(00)00711-3.

[94] A. Cortés, R. Lavin, J. C. Denardin, R. E. Marotti, E. A. Dalchiele, P. Valdivia, and Humberto Gómez, Template assisted electrochemical growth of cobalt nanowires: Influence of deposition conditions on structural, optical and magnetic properties, *J. Nanosci. Nanotechnol.*, 2011, 11, 3899–3910, doi: 10.1166/jnn.2011.3826.

[95] J. Sánchez-Barriga, M. Lucas, G. Rivero, P. Marin, and A. Hernando, Magnetoelectrolysis of Co nanowire arrays grown in a track-etched polycarbonate membrane, *J. Magn. Magn. Mater.*, 2007, 312, 99–106, doi: 10.1016/j.jmmm.2006.09.020.

[96] F. Li, T. Wang, L. Ren, and J. Sun, Structure and magnetic properties of Co nanowires in self-assembled arrays, *J. Phys. Condens. Matter*, 2004, 16, 8053–8060, doi: 10.1088/0953-8984/16/45/027.

[97] D. Navas, K. R. Pirota, P. Mendoza Zelis, D. Velazquez, C. A. Ross, and M. Vazquez, Effects of the magnetoelastic anisotropy in Ni nanowire arrays, *J. Appl. Phys.*, 2008, 103, 103–106, doi: 10.1063/1.2834719.

[98] K. Nielsch, R. B. Wehrspohn, J. Barthel, J. Kirschner, U. Gösele, S. F. Fischer, and H. Kronmüller, Hexagonally ordered 100 nm period nickel nanowire arrays, *Appl. Phys. Lett.*, 2001, 79, 1360–1362, doi: 10.1063/1.1399006.

[99] J. I. Schwerdt, G. F. Goya, M. P. Calatayud, C. B. Hereñú, P. C. Reggiani, and R. G. Goya, Magnetic field-assisted gene delivery: achievements and therapeutic potential., *Curr. Gene Ther.*, 2012, 12, 116–26, doi: 10.2174/156652312800099616.

[100] J. Wang, J. Li, J. Wang, F. Bu, H. Kou, C. Li, P. Zhang and Eric Beaugnon, Effect of solidification on microstructure and properties of FeCoNi(AlSi)0.2 high-entropy alloy under strong static magnetic field, *Entropy*, 2018, 20, 275-12, doi: 10.3390/e20040275.

[101] D. J. Sellmyer, M. Zheng, and R. Skomski, Magnetism of FE, CO and NI nanowires in self-

assembled arrays, *J. Phys. Condens. Matter*, 2001, 13, R460-29, doi: 10.1088/0953-8984/13/25/201.